Black Hole Growth and Feedback in Isolated ROMULUS25 Dwarf Galaxies

Ray S. Sharma[1] , Alyson M. Brooks[1] , Rachel S. Somerville[2], Michael Tremmel[3] , Jillian Bellovary[4,5,6] ,
Anna C. Wright[1], and Thomas R. Quinn[7]
[1] Department of Physics and Astronomy, Rutgers, The State University of New Jersey, 136 Frelinghuysen Road, Piscataway, NJ 08854, USA
[2] Simons Center for Computational Astrophysics, New York, NY 10010, USA
[3] Department of Astronomy, Yale University, 52 Hillhouse Avenue, New Haven, CT 06511, USA
[4] Department of Physics, Queensborough Community College, City University of New York, 222–05 56th Avenue, Bayside, NY 11364, USA
[5] Department of Astrophysics, American Museum of Natural History, Central Park West at 79th Street, New York, NY 10024, USA
[6] The Graduate Center, City University of New York, 365 5th Avenue, New York, NY 10016, USA
[7] Department of Astronomy, University of Washington, P.O. Box 351580, Seattle, WA 98195, USA
Received 2019 December 5; revised 2020 May 18; accepted 2020 May 22; published 2020 July 7

Abstract

We investigate the effects of massive black hole growth on the structural evolution of dwarf galaxies within the ROMULUS25 cosmological hydrodynamical simulation. We study a sample of 205 central, isolated dwarf galaxies with stellar masses $M_{star} < 10^{10} M_{\odot}$ and a central BH. We find that the local M_{BH}–M_{star} relation exhibits a high degree of scatter below $M_{star} < 10^{10} M_{\odot}$, which we use to classify BHs as overmassive or undermassive relative to their host M_{star}. Within isolated dwarf galaxies, only 8% of undermassive BHs ever undergo a BH merger, while 95% of overmassive BHs grow through a mixture of BH mergers and accretion. We find that isolated dwarf galaxies that host overmassive BHs also follow different evolutionary tracks relative to their undermassive BH counterparts, building up their stars and dark matter earlier and experiencing star formation suppression starting around $z = 2$. By $z = 0.05$, overmassive BH hosts above $M_{star} > 10^9 M_{\odot}$ are more likely to exhibit lower central stellar mass density, lower H I gas content, and lower star formation rates than their undermassive BH counterparts. Our results suggest that overmassive BHs in isolated galaxies above $M_{star} > 10^9 M_{\odot}$ are capable of driving feedback, in many cases suppressing and even quenching star formation by late times.

Unified Astronomy Thesaurus concepts: Supermassive black holes (1663); N-body simulations (1083); Dwarf galaxies (416); Black hole physics (159)

1. Introduction

Evidence has built over the past two decades demonstrating that massive black holes (BHs) are ubiquitous in massive galaxies (Kormendy & Richstone 1995; Kormendy & Ho 2013) though less common in low-mass galaxies (Shields et al. 2008; Reines et al. 2013; Moran et al. 2014). BHs in massive galaxies are thought to coevolve with their host through a number of processes connecting BH growth to host growth (Fabian 2012; Heckman & Best 2014; Somerville & Davé 2015). There are numerous detections of active galactic nuclei (AGN) within dwarf galaxies (Reines et al. 2013; Lemons et al. 2015; Reines & Volonteri 2015; Pardo et al. 2016; Baldassare et al. 2017; Ahn et al. 2018; Baldassare et al. 2018, 2020; Martín-Navarro & Mezcua 2018). Recent studies have also estimated dynamical masses for many weakly accreting BHs within dwarf galaxies (Reines & Volonteri 2015; Nguyen et al. 2017, 2018, 2019, 2020). However, studying the role that BHs play in the evolution of dwarf galaxies has only become possible in recent years.

Massive BHs have been observed to have a significant impact on gas and stars within dwarf galaxies. Penny et al. (2018) identify six dwarf galaxies ($M_{star} < 5 \times 10^9 M_{\odot}$) within the Sloan Digital Sky Survey (SDSS) that exhibit (1) kinematically offset stars and ionized gas components and (2) strongly AGN-like emission line ratios identifying the AGN as the primary source of gas ionization. Manzano-King et al. (2019) identify nine SDSS dwarf galaxies with AGN-like narrow-line emission and indirect evidence of AGN-driven star formation suppression. Bradford et al. (2018) find evidence of reduced H I gas mass in isolated dwarf galaxies ($10^{9.2} M_{\odot}$

$< M_{star} < 10^{9.5} M_{\odot}$) exhibiting AGN-like ionizing radiation, using H I-selected data from ALFALFA and optically selected data from SDSS. Similarly, Dickey et al. (2019) find a connection between AGN-like ionizing radiation and quenching of star formation in the host galaxy, using Keck/ESI spectra of isolated dwarf galaxies ($10^9 < M_{star} < 10^{9.5} M_{\odot}$). Silk (2017) find, within the dense progenitors of modern dwarf galaxies, that BHs can generate an order of magnitude more power than supernovae (SNe). Silk argues that early BH feedback may play a role in explaining a number of problems in modeling structure formation, such as suppression of luminous dwarf formation (Trujillo-Gomez et al. 2015), the missing cold baryons in the local universe (Bregman et al. 2015), and the source of ionizing photons during reionization (Madau & Haardt 2015).

Although observations indicate that BHs may impact dwarf galaxy evolution, detecting BHs and disentangling the precise role of BHs in dwarf galaxies is difficult for a few reasons. First, the sample sizes involved in surveys of BHs in dwarf galaxies may be restricted by the fraction of galaxies that host BHs (Greene 2012). We define the BH occupation fraction to be the total number of BH-hosting galaxies compared to the total number of galaxies, for a given stellar mass. Recent work finds that the BH occupation fraction is sensitive to the BH formation mechanism (Ricarte & Natarajan 2018) and may drop to zero for sufficiently low-mass galaxies. Observations are consistent with a roughly 100% occupation fraction down to $M_{star} \sim 10^9 M_{\odot}$ (Miller et al. 2015; Nguyen et al. 2018, 2019; Baldassare et al. 2020). Simulations suggest that the BH occupation fraction plummets below stellar mass $M_{star} < 10^9 M_{\odot}$ (Habouzit et al. 2017; Ricarte & Natarajan 2018; Bellovary et al. 2019).

Measuring the true BH occupation fraction is further restricted by the difficulties in detecting weakly accreting BHs outside of the local universe (Bellovary et al. 2019).

Second, detection of BH-induced star formation suppression is impeded by evidence that low-mass galaxy quenching in group environments is closely tied to tidal effects (Penny et al. 2016). Over 99% of quenched dwarf galaxies seem to be found within 1.5 Mpc of a galaxy with Milky Way mass or greater (Geha et al. 2012). Although AGNs may be more easily observed in group environments than in the field (Penny et al. 2018), distinguishing the dominant quenching source within groups proves challenging.

Third, BH detection surveys often suffer from dust obscuration and sample contamination from various sources. A large portion of AGNs in dwarf galaxies may be completely missed in optical or X-ray surveys owing to heavy dust obscuration (Chen et al. 2017; Liu et al. 2018). X-ray binaries can further contaminate surveys that identify AGNs through X-ray detection (Yuan et al. 2014; Miller et al. 2015). The effects of star formation and BH accretion on ionizing the interstellar medium (ISM) are difficult (if not impossible) to disentangle in low-metallicity galaxies (Groves et al. 2006; Kewley et al. 2013). Reines et al. (2013) find that identifying AGNs solely through ionizing radiation diagnostics can lead to missed detections.

The difficulties in detecting BHs and disentangling their impact necessitate the use of simulations to further study them. High-resolution cosmological simulations provide one of the best laboratories for predicting BH population growth and behavior, over a wide range of host stellar masses and redshifts. In the past few years, simulations have successfully begun to reach the resolutions required to capture BH physics within low-mass galaxies. Habouzit et al. (2017) find that SN feedback within simulated low-mass SUPERCHUNKY galaxies ($M_{\rm halo} \lesssim 10^{10.5} M_{\odot}$) can suppress accretion onto the central BH. By modeling AGN and SN outflows, Dashyan et al. (2018) suggest that extended periods of BH growth and activity can drive gas out of dwarf galaxies more efficiently than SNe. Cosmological simulations run by Barai & de Gouveia Dal Pino (2019) find that BHs are capable of quenching dwarf galaxies through BH feedback by $z = 4$. Using high-resolution, cosmological, zoom-in simulations, Bellovary et al. (2019) constrain the cosmic BH occupation fraction in low-mass galaxies and find that BHs within dwarf galaxies grow little throughout their lifetime. Koudmani et al. (2019) test various models of AGN feedback in simulated dwarf galaxies, finding that AGNs can significantly enhance outflow temperatures and velocities from stellar processes, inhibiting gas inflows.

Simulations that include BHs face a number of numerical obstacles. Simulating BH growth and feedback requires simulating a large range of scales with high resolution. To mitigate these limitations, simulations incorporate subgrid prescriptions designed to model physics occurring below the resolution limits. Subgrid prescriptions have been shown to reproduce observed properties of BHs and their hosts (Hirschmann et al. 2014; Sijacki et al. 2014; Volonteri et al. 2016; Habouzit et al. 2017, 2019). However, the chosen prescriptions for BH formation, dynamics, and accretion can drastically impact the predicted BH growth, occupation fraction, and assembly history of the galaxy (Ricarte & Natarajan 2018). Furthermore, the especially high resolutions required to capture

BH physics in dwarf galaxies force most cosmological simulations to set a halo mass threshold for BH formation.

In this paper we analyze results from the high-resolution ROMULUS25 cosmological simulation to understand how BHs in dwarf galaxies grow and interact with their environments. We explore the growth mechanisms and evolutionary history of BHs, the connection between BH growth and host galaxy growth, and the possibility of significant BH feedback in ROMULUS25 dwarf galaxies. ROMULUS25 is well suited for this analysis since it is currently the only cosmological simulation capable of forming BHs in low-mass galaxies at high enough resolution and with sufficiently detailed physical prescriptions to accurately track their dynamics and growth (see Section 2.3 for details). To model the evolution of BHs, simulations must be able to accurately account for dynamical friction, which requires dark matter and stars at higher mass resolution than BHs to realistically model BH dynamics (Tremmel et al. 2015). Hence, the BH seed mass in ROMULUS25 is closely tied to the simulation resolution. ROMULUS25 achieves BHs that are ~3 times more massive than dark matter particles, while also being one of the highest-resolution simulation volumes to date. Additionally, while most simulations set a halo mass threshold for BH formation, ROMULUS25 does not have a priori assumption of the BH occupation fraction. Our analysis also gives insight into how the BH physics and subgrid recipes within ROMULUS25 affect BH growth in dwarf galaxies.

In Section 2 we describe the physics of the ROMULUS25 - cosmological simulation. In Section 3 we explore the connection between BH growth and properties of the host dwarf galaxy. In particular, we explore how dwarf galaxies can form significantly overmassive and undermassive BHs, and how such BHs may drive evolutionary differences between their hosts. We discuss the consequences of scatter in the $M_{\rm BH}$–$M_{\rm star}$ relation, as well as the impact of BHs on star and gas properties in dwarf galaxies.

2. ROMULUS Simulation Suite

2.1. Simulation Properties

The ROMULUS suite of cosmological simulations was run using the Tree+SPH code ChaNGa (Menon et al. 2015), which inherits baryonic prescriptions from GASOLINE and GASOLINE2 (Wadsley et al. 2004, 2008; Stinson et al. 2006; Shen et al. 2010; Wadsley et al. 2017). In this work we analyze ROMULUS25, the 25 Mpc-per-side uniform box with periodic boundary conditions. We analyze ROMULUS25 because of its large, uniform sample of low-mass galaxies with BHs run to $z = 0$.

ROMULUS25 has comparable mass resolution to recent cosmological simulations such as ILLUSTRISTNG (Springel et al. 2018) and Horizon-AGN (Volonteri et al. 2016), as well as force resolution comparable to the highest-resolution runs of EAGLE (Schaye et al. 2015). ROMULUS25 resolves gravity with a Plummer equivalent force softening of $\epsilon_g = 250$ pc. Typically, the number of gas particles in a simulation is equal to the number of dark matter particles, while the relative masses are set according to the cosmic baryon fraction. ROMULUS25 instead contains 3.375× more dark matter particles than gas particles, with dark matter particles of mass $3.39 \times 10^5 M_{\odot}$ and gas particles of mass $2.12 \times 10^5 M_{\odot}$. This "oversampling" of dark matter provides ROMULUS25 with better-resolved BH

dynamics (Tremmel et al. 2015). The ROMULUS suite of simulations was run with a Planck 2014 ΛCDM cosmology, with $\Omega_m = 0.3086$, $\Omega_\Lambda = 0.6914$, $h = 0.6777$, and $\sigma_8 = 0.8288$ (Planck Collaboration et al. 2014).

Halos were identified using the AMIGA Halo Finder (Knollmann & Knebe 2009) and analyzed using the simulation analysis code PYNBODY (Pontzen et al. 2013). Key properties were organized into a TANGOS database (Pontzen & Tremmel 2018).

We calculate halo mass, M_{200}, such that

$$M_{200} = 4\pi\rho_c \Delta_h R_{200}^3, \tag{1}$$

where ρ_c is the critical density, $\Delta_h = 200$ is the overdensity threshold, and R_{200} is the halo radius.

Star formation in ROMULUS25 is regulated by the star formation efficiency, the efficiency of SN energy injection into the ISM, and the density/temperature threshold beyond which stars are allowed to form. SN feedback follows the blast wave prescription from Stinson et al. (2006).

Parameters governing star formation were constrained based on a series of 80 "zoom-in" (Governato et al. 2009) simulations of four galaxies with halo masses $10^{10.5}$–$10^{12}M_\odot$, run without BH physics, with the aim of reproducing a set of observed $z = 0$ scaling relations for galaxies. The parameter spaces were explored using the Kriging algorithm and graded by agreement with the stellar mass–halo mass relation (Moster et al. 2013); the relationship between stellar mass, angular momentum, and morphology (Obreschkow & Glazebrook 2014); and the H I gas–stellar mass relation (Cannon et al. 2011; Haynes et al. 2011). The Kriging algorithm efficiently traverses the parameter space and penalizes parameter selections that lead to deviations from the observed scaling relations. The parameters governing BH growth were afterward constrained in a similar fashion (see Section 2.4). ROMULUS25 adopts the following:

1. SF efficiency, $c_* = 0.15$.
2. Gas density threshold, $n_* = 0.2 m_p$ cm^{-3}.
3. SN coupling efficiency, $\epsilon_{SN} = 0.75$.

ROMULUS25 incorporates prescriptions for metal and thermal diffusion from Shen et al. (2010) and Governato et al. (2015) and low-temperature radiative cooling as in Guedes et al. (2011). The SN feedback is based on a Kroupa (2001) initial mass function. Specifics of the physics and calibration process for ROMULUS25 are detailed in Tremmel et al. (2017).

2.2. Black Hole Seeding

Simulations commonly seed BHs by choosing a halo mass threshold above which galaxies are allowed to form a BH (Sijacki et al. 2014; Anglés-Alcázar et al. 2017). BHs are then formed from star-forming gas and placed in the halo center (Agarwal et al. 2014). Instead, ROMULUS25 seeds BHs based on conditions of the pre-collapse gas using characteristics of direct-collapse seeding (Haiman 2013). In this work we qualitatively define massive BHs as BHs with masses relevant to direct-collapse seeding models ($M_{BH} \gtrsim 10^5 M_\odot$). ROMULUS25 seeds massive BHs at high redshift ($z \gtrsim 5$) without assumptions of the BH occupation fraction. A gas particle is marked to form a BH if it has the following:

1. Low metallicity, $Z < 3 \times 10^{-4}$.
2. High density, $15\times$ higher than the SF threshold.
3. Temperature between 9500 and 10,000 K.

In other words, a gas particle will form a BH if the gas is set to collapse quickly and cool slowly, following predicted sites of direct-collapse seeding (Begelman et al. 2006; Johnson et al. 2012; Volonteri 2012; Haiman 2013; Reines & Comastri 2016). In particular, a low metallicity threshold prevents premature gas fragmentation and pushes seed formation to early times when gas has undergone little metal enrichment (Greene 2012). The values were chosen to restrict BH growth to the highest-density regions in the early universe, where BHs can undergo rapid accretion. Choosing lower metallicity or colder temperature thresholds was found to bias formation away from the densest regions (Tremmel et al. 2017).

Once these gas conditions are met, a BH is seeded at a mass of $M_{BH} = 10^6 M_\odot$. Seeding accretes mass from nearby gas particles to conserve total mass and simulate rapid, unresolved growth thought to exceed $0.1 M_\odot$ yr^{-1} (Hosokawa et al. 2013; Schleicher et al. 2013). This seed mass is high relative to some other simulations, such as ILLUSTRISTNG (Nelson et al. 2019). Dynamical BH estimates (e.g., Nguyen et al. 2019) also indicate that BHs in dwarf galaxies can fall to masses well below $10^6 M_\odot$. However, seeding BHs at a higher mass ensures that both BH dynamics and gas accretion are well resolved throughout their lifetimes (Tremmel et al. 2015). Further, the formation mechanism ensures that BHs are only seeded in regions with dense, collapsing gas that is unlikely to form stars, and hence are more likely to grow BHs rapidly. For more detailed caveats related to the BH seeding mechanism, see Section 3.5.

2.3. Black Hole Dynamics

Dynamical friction between BHs and their hosts causes BHs to sink toward the galaxy center (Kazantzidis et al. 2005; Pfister et al. 2017). Dynamical friction interactions occur at both large scales (Colpi et al. 1999) and scales below the resolution of most cosmological simulations. Common practice in cosmological simulations is to reposition the BH along local potential gradients as it begins to migrate, forcefully recentering it. However, this method suppresses BH motion around the galaxy and artificially inflates BH growth rates (Tremmel et al. 2017). ROMULUS25 instead incorporates a dynamical friction subgrid recipe shown to reproduce realistic BH sinking timescales. This recipe allows BHs to naturally "wander" within galaxies (Tremmel et al. 2018; Bellovary et al. 2019; Reines et al. 2020). Tremmel et al. (2015) find that the spatial resolution in ROMULUS25, combined with its oversampling of dark matter, also avoids unrealistic numerical heating of BHs found in lower-resolution simulations.

Assuming an isotropic velocity distribution of particles within a gravitational softening length, ϵ_g, from the BH, we can write the acceleration due to dynamical friction (Chandrasekhar 1943):

$$a_{DF} = -4\pi G^2 M_{BH} \rho(<v_{BH}) \ln\Lambda \frac{v_{BH}}{v_{BH}^3}, \tag{2}$$

where M_{BH} is the mass of the BH, $\rho(<v_{BH})$ is the density of nearby particles moving slower than the BH, $\ln\Lambda$ is the Coulomb logarithm, and v_{BH} is the velocity of the BH. Velocities are calculated relative to the local center of mass within the smoothing kernel. The Coulomb logarithm is approximated by $\ln\Lambda \sim \ln\frac{b_{max}}{b_{min}}$, where b_{max} and b_{min} are, respectively, the maximum and minimum impact parameters of

the surrounding particles. The maximum impact parameter is restricted to $b_{max} = \epsilon_g$ to avoid double counting of resolved dynamical frictional forces. The minimum impact parameter is restricted to the 90° deflection radius with a lower limit of the Schwarzschild radius of the BH. Acceleration is calculated from the nearest 64 collisionless particles. Mergers occur when BHs fall within $2\epsilon_g$ of one another and have low enough relative velocity to be considered gravitationally bound.

2.4. Black Hole Accretion and Feedback

BH accretion is handled through a Bondi–Hoyle prescription modified to incorporate angular momentum support on resolved scales. The accretion rate is driven by mass flux across a resolved accretion radius, defined as the radius where gravitational potential balances with the minimally resolved thermal energy of the surrounding gas. Accretion rates are averaged over the smallest simulation time step at a given time, typically $10^4–10^5$ yr. We can write the accretion rate depending on whether the dominant gas motion is rotational, v_θ, or bulk flow, v_{bulk}:

$$\dot{M} = \alpha \times \begin{cases} \dfrac{\pi G^2 M_{BH}^2 \rho}{(v_{bulk}^2 + c_s^2)^{3/2}} & \text{if } v_{bulk} > v_\theta \\[2ex] \dfrac{\pi G^2 M_{BH}^2 \rho c_s}{(v_\theta^2 + c_s^2)^2} & \text{if } v_{bulk} < v_\theta, \end{cases} \quad (3)$$

where

$$\alpha = \begin{cases} \left(\dfrac{n_{gas}}{n_*}\right)^\beta & \text{if } n_{gas} \geqslant n_* \\[2ex] 1 & \text{if } n_{gas} \leqslant n_*, \end{cases}$$

is the density-dependent boost factor that corrects for under-estimates of accretion rate due to resolution limitations (Booth & Schaye 2009), $\beta = 2$ is the corresponding boost coefficient, n_{gas} is the number density of the surrounding gas, n_* is the star formation density threshold, ρ is the mass density of the surrounding gas, c_s is the local sound speed, v_θ is the rotational velocity of the surrounding gas at the smallest resolved scales, and v_{bulk} is the bulk velocity of the surrounding gas. This calculation is performed over the 32 nearest particles. BH accretion in ROMULUS25 is Eddington limited.

BH feedback is handled through a subgrid recipe similar to the blast wave SN feedback model. Thermal energy from accretion is isotropically transferred to the nearest 32 gas particles, weighted by the SPH kernel. To ensure realistic dissipation of feedback energy, gas particles that receive energy are stopped from cooling for roughly the gas dynamical time step over which the accretion is calculated (Tremmel et al. 2017). The energy coupled to the surrounding gas is

$$E = \epsilon_r \epsilon_f \dot{M} c^2 dt, \quad (4)$$

where $\epsilon_r = 0.1$ is the assumed radiative efficiency of the BH and $\epsilon_f = 0.02$ is the coupling efficiency of the thermal energy to the surrounding gas (see below). This form of BH feedback has been shown to efficiently quench galaxies with halo masses above a few $\times 10^{11} M_\odot$ (Pontzen et al. 2017).

The accretion efficiency, β, and coupling efficiency, ϵ_f, were constrained through 48 zoom-in simulations of the same four

Table 1
Sample Sizes of Isolated Galaxies in ROMULUS25 with and without Massive BHs, Distinguishing between BH Classifications

Sample	All M_{star}	$10^8 < M_{star} < 10^{10} M_\odot$
Undermassive	78	52
Median	150	99
Overmassive	78	54
With BHs	306	205
Without BHs	267	197

galaxies used for constraining star formation parameters, run with BH physics. The star formation parameters were left unchanged from the initial parameter search, and instead the BH parameters were allowed to change. The parameter space was explored using the Kriging algorithm and graded by agreement with an empirical $z = 0$ BH mass–stellar mass relation (Schramm & Silverman 2013). The results of this parameter search were also used in the high-resolution cosmological hydrodynamic, galaxy cluster simulation, ROMU-LUSC (Tremmel et al. 2019).

3. Results

We restrict our sample in a few ways. We select galaxies with stellar masses between $10^8 M_\odot < M_{star} < 10^{10} M_\odot$ at $z = 0.05$, where the lower threshold ensures that galaxies have at least several hundred star particles. We also restrict our sample to central, relatively isolated galaxies to better separate the effects of BHs from the effects of group environments on dwarf galaxy evolution. A halo is considered isolated if it is farther than one halo radius R_{200} from another halo of equal or greater mass at $z = 0$. Following Geha et al. (2012), galaxies below $M_{star} < 10^{10} M_\odot$ must be farther than 1.5 Mpc from a galaxy with $M_{star} > 2.5 \times 10^{10} M_\odot$ to be considered isolated. Geha et al. find evidence of environmental quenching of low-mass galaxies within such scales, although they focused on galaxies with $M_{star} < 10^9 M_\odot$. Since many BHs have been found in dwarfs between $10^9 M_\odot < M_{star} < 10^{10} M_\odot$, we study the full range of ROMULUS25 dwarfs up to $M_{star} < 10^{10} M_\odot$ but still apply the isolation criteria above. Finally, we define the central BH to be the most massive BH within 2 kpc of the halo center, since ROMULUS25 halos can contain many BHs at varying radii from the center (Tremmel et al. 2018). Once we restrict to only hosts of central BHs, the mean BH distance for our galaxy sample drops from 1 kpc to 170 pc.

These restrictions give us a sample of 205 isolated dwarf galaxies with central BHs, as well as a sample of 197 isolated dwarf galaxies entirely without BHs. We summarize our sample sizes in Table 1, alongside sample sizes for specific subsets of our data (see Section 3.1 for details).

We use stellar mass corrections from Munshi et al. (2013) that account for the impact of aperture photometry on observed stellar masses. These corrections allow us to perform a more "apples-to-apples" comparison between simulated and observed stellar masses. Following Munshi et al., we correct stellar masses such that $M_{star,obs} = 0.6 M_{star,sim}$.

3.1. M_{BH}–M_{star} Relation

Figure 1 shows the $z = 0.05$ M_{BH}−M_{star} relation for all isolated ROMULUS25 galaxies with central BHs. Galaxies below $M_{star} < 10^{10} M_\odot$ exhibit a high degree of scatter in
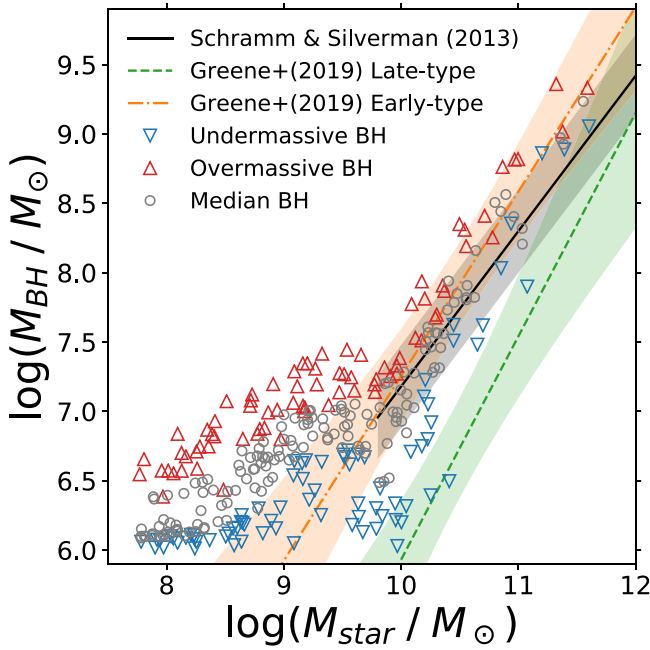
Figure 1. The $z = 0.05$ BH mass vs. stellar mass relation for all isolated galaxies in ROMULUS25 with central BHs. The relation has large scatter in M_{BH} below $M_{star} < 10^{10} M_{\odot}$ but becomes well constrained above $M_{star} > 10^{10} M_{\odot}$. Galaxies are colored according to whether the hosted BH is overmassive (red triangles), undermassive (blue inverted triangles), or median (gray circles) (see text for definitions). We compare our relation to both the early-type (orange dashed–dotted) and late-type (green dashed) relations compiled by Greene et al. (2019), as well as the X-ray-selected broad-line AGN relation from Schramm & Silverman (2013) (black solid). Shaded regions indicate 1σ observational uncertainties. Above $M_{star} \gtrsim 10^{10} M_{\odot}$, ROMULUS25 shows agreement with the relation from Schramm & Silverman, as well as with the early-type relation from Greene et al. Below $M_{star} < 10^{10} M_{\odot}$, the total BH mass is dominated by the BH seed mass and we find significant deviation away from observed relations.

M_{BH}, which is a phenomenon that has been predicted and observed before. Using semianalytic models, Volonteri & Natarajan (2009) find that the evolution of BHs toward the local $M_{BH} - \sigma$ relation is dependent on both the BH growth history and seed BH mass. They find that low-mass BHs exhibit a higher amount of scatter on the $M_{BH} - \sigma$ relation than higher-mass BHs. Using cosmological hydrodynamical simulations, Barai & de Gouveia Dal Pino (2019) similarly find high scatter in the $M_{BH} - M_{star}$ relation at low stellar masses. Reines & Volonteri (2015) find that the $M_{BH} - M_{star}$ relation observed in high-mass galaxies breaks down in low-mass galaxies. They find that low-mass star-forming galaxies may instead follow a relation with lower BH masses than expected. In high-mass galaxies, Shankar et al. (2016) find that dynamical estimates of the local $M_{BH} - M_{star}$ relation are biased by the requirement that the BH sphere of influence be fully resolved. Shankar et al. find that corrections to this bias place dynamical $M_{BH} - M_{star}$ relations in closer agreement with AGN-derived relations and eliminate much of the perceived scatter in M_{BH} at high M_{star}.

Galaxies around $M_{star} \sim 10^8 M_{\odot}$ tend to clump up at the BH seed mass and twice the seed mass. The simulation BH seeding mechanism introduces a floor that likely inflates BH masses in the lightest dwarf galaxies relative to observations. We do not remove hosts of seed mass BHs from the sample since it is unclear what additional biases would be introduced relative to a higher-resolution seeding mechanism. For some analyses that

follow we separate the sample into two mass bins since resolution may impact results at the lowest masses.

We compare with observed relations from Schramm & Silverman (2013; SS13) and Greene et al. (2019). ROMULUS25 agrees with the Greene et al. relation for early-type galaxies at stellar masses $M_{star} > 10^{10} M_{\odot}$, as well as with the SS13 relation. Above $M_{star} \gtrsim 10^{10} M_{\odot}$, galaxies follow the SS13 relation in part because the BH physics is tuned to match with the low-mass end of the SS13 relation. For similar reasons, ROMULUS25 does not agree with the Greene et al. relation for late-type galaxies.

The divergence between the various relations may be due to a mixture of a few effects: morphological differences in the host galaxy, differences in accretion efficiencies between BHs, and uncertainties in observational BH mass estimators. Reines & Volonteri (2015) find significant differences between their $M_{BH} - M_{star}$ relations for bulge-dominated galaxies and AGNs. Their bulge-dominated galaxy sample has dynamical BH mass estimates, while their AGN sample contains a mixture of pseudobulges and classical bulges with broad Hα virial + reverberation-mapped BH masses. They find that the scatter in the combined $M_{BH} - M_{star}$ relation is closely related to the morphology of the host galaxy, where bulge-dominated galaxies sit on a relation with similar slope but higher normalization than spiral galaxies. SS13 do not make morphological distinctions in their sample and base their relation on X-ray-selected AGNs with broad Mg II virial BH masses. Similarly, Davis et al. (2018) find that late-type galaxies follow a steeper $M_{BH} - M_{star}$ relation than early-type galaxies down to $M_{star} \sim 10^{10.5} M_{\odot}$, which Sahu et al. (2019) find is fundamentally a difference in bulge morphology of the host galaxies.

Trump et al. (2011) find that broad emission line regions are only observed in rapidly accreting AGNs with luminosities greater than $10^{-2} L_{Edd}$, where L_{Edd} is the Eddington luminosity. By analyzing ROMULUS25, Ricarte et al. (2019) find that high Eddington ratios are associated with BHs that exhibit systematically lower masses than expected for their host stellar mass.

Indirect measurements of BH masses within AGNs are typically thought to yield large uncertainties, dependent on their luminosity and redshift (e.g., Shen & Kelly 2012; Kelly & Shen 2013). Virial BH mass estimates of AGNs require assumptions of the geometry and orientation of the broad-line region (Denney et al. 2010; Barth et al. 2011) and may be biased by nongravitational contributions to broad-line widths (Krolik 2001). However, Reines & Volonteri (2015) argue that the difference between $M_{BH} - M_{star}$ relations for AGNs and elliptical galaxies is far larger than can be explained by uncertainties in virial BH masses. They further find that their virial BH masses would need an unreasonably high virial factor in order to match the elliptical galaxy relation.

We quantify scatter in the $M_{BH} - M_{star}$ relation by the residual away from the median M_{BH} in bins of M_{star}. Within each bin we classify BHs with masses in the bottom 25% as "undermassive," while BHs within the top 25% are classified as "overmassive." BHs falling between the two quartiles are classified as "median." We summarize our sample sizes in Table 1. We show this classification scheme at all stellar masses, though the classification is most meaningful in dwarf galaxies where the central BHs show a high degree of scatter in M_{BH}. A similar classification scheme is built by Li et al. (2020) for $M_{star} > 10^{10} M_{\odot}$ ILLUSTRIS galaxies and $M_{star} > 10^9 M_{\odot}$
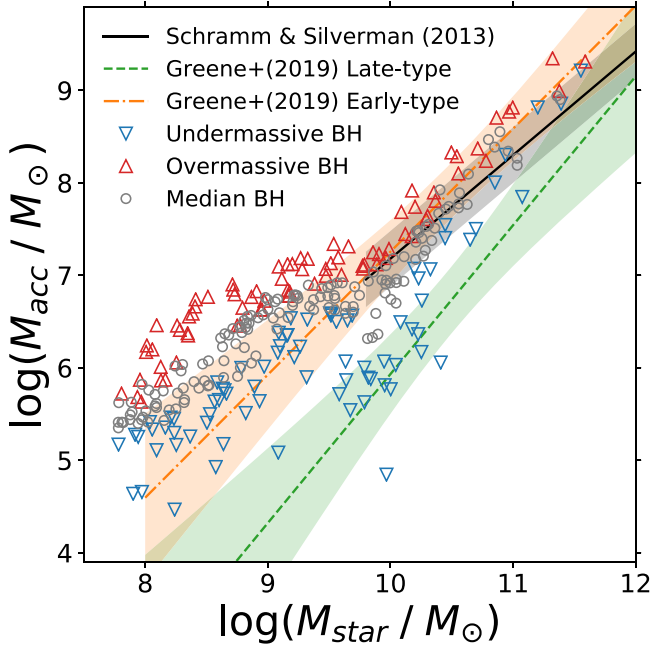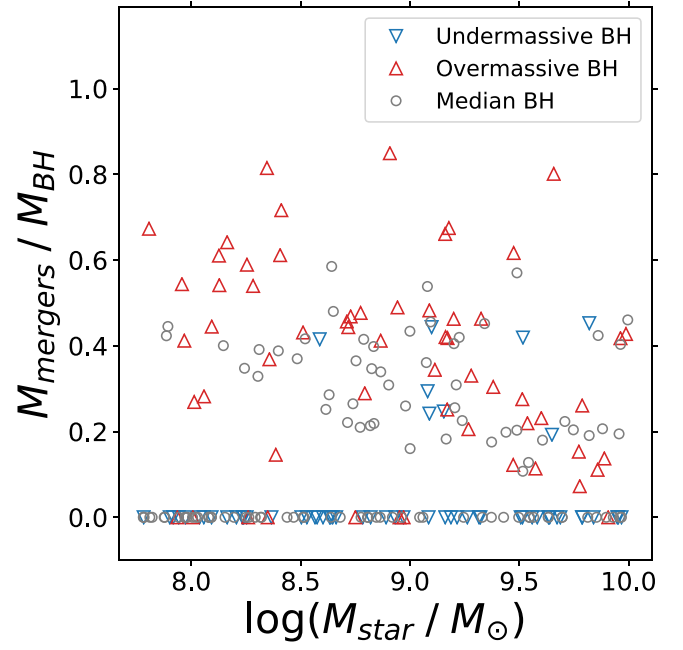
Figure 2. The $z = 0.05$ total accreted BH mass vs. stellar mass relation for all isolated galaxies in ROMULUS25 with central BHs. The relation has large scatter in M_{acc} below $M_{star} < 10^{10} M_\odot$, as in Figure 1. Galaxies are colored according to whether the hosted BH is overmassive (red triangles), undermassive (blue inverted triangles), or median (gray circles). ROMULUS25 shows agreement with the relation from Schramm & Silverman (2013), as well as with the early-type relation from Greene et al. (2019). Below $M_{star} < 10^{10} M_\odot$, overmassive BHs tend to fall above the early-type relation.

Figure 3. Fractional growth of BHs through mergers vs. stellar mass, at $z = 0.05$. Galaxies are colored by whether the BH is overmassive (red triangles), undermassive (blue inverted triangles), or median (gray circles). Nearly all undermassive BHs grow solely through accretion onto the main progenitor, never having experienced a BH merger. Overmassive and many median BHs grow through a combination of mergers and accretion onto the main progenitor. BHs in hosts with stellar masses $M_{star} \lesssim 10^9 M_\odot$ tend to have their growth dominated by mergers, while those in higher-mass hosts tend to be dominated by accretion onto the main progenitor.

TNG100 galaxies, though they instead define overmassive and undermassive BHs on the $M_{BH}-\sigma$ relation.

It should be emphasized that current observations find that BHs in dwarf galaxies can have masses lower than the resolution limit of ROMULUS25. Baldassare et al. (2015) find a BH in the dwarf galaxy RGG 118 with a virial mass of $M_{BH} = 5 \times 10^4 M_\odot$. Nguyen et al. (2017) calculate a dynamical BH mass of $M_{BH} = 1.5 \times 10^5 M_\odot$ in the nearby dwarf galaxy NGC 404. Nguyen et al. (2019) improve dynamical BH masses for three nearby low-mass galaxies, where all three show BH masses below 1 million solar masses and one shows a dynamical mass of $M_{BH} = 6.8 \times 10^3 M_\odot$. Graham & Soria (2019) and Graham et al. (2019) use BH scaling relations to predict BH masses as low as $M_{BH} \sim 10^4 M_\odot$ in low-mass galaxies in the Virgo Cluster.

Following Ricarte et al. (2019), we can partially compensate for the effects of the BH seeding mechanism and define the total mass a given BH has grown via accretion, M_{acc}. This definition completely excludes the contributions of BH seeding and only counts accretion onto every progenitor within the BH merger tree. We are able to trace M_{acc} well below the BH seed mass because of the high resolution of gas accretion in ROMULUS25. Figure 2 shows the $M_{acc}-M_{star}$ relation for all isolated ROMULUS25 galaxies with central BHs, compared with observed $M_{BH}-M_{star}$ relations. We find that the $M_{acc}-M_{star}$ relation continues linearly below the BH seed mass and shows better agreement with the observed relations. Galaxies below $M_{star} < 10^{10} M_\odot$ still show a high degree of scatter in M_{acc}, while higher mass galaxies do not. Overmassive BHs in galaxies below $M_{star} < 10^{10} M_\odot$ tend to fall above the observed relations. Notably, BHs that are considered overmassive or undermassive in M_{BH} are typically overmassive or

undermassive in M_{acc} as well. Although it is unclear how much the BH seed mass affects growth, ROMULUS25 is capable of producing many BHs with growth consistent with current observational constraints by $z = 0.05$.

3.2. BH Growth Modes

Understanding the source of scatter in the $M_{BH}-M_{star}$ relation requires first understanding how the BHs evolved to the present day. BHs grow through BH–BH mergers, as well as through accretion of gas particles. We trace the growth history of each BH and calculate the growth through mergers onto the main progenitor, $M_{mergers}$.

Figure 3 shows the fraction of total BH mass grown via mergers by $z = 0.05$ versus the host stellar mass. By $z = 0.05$, only 8% of undermassive BHs have ever undergone a BH merger, and instead the vast majority grow solely through accretion. On the other hand, 95% of overmassive BHs have undergone at least one BH merger and grow through a mixture of BH mergers and accretion at higher rates than undermassive BHs. The primary mode of growth for overmassive BHs depends on host stellar mass, where those found in hosts below $M_{star} \lesssim 10^9 M_\odot$ grow primarily through BH mergers and those found in hosts above $M_{star} \gtrsim 10^9 M_\odot$ grow primarily through accretion onto the main BH progenitor.

We next turn to how BHs evolve relative to the stellar mass of their hosts. Figure 4 shows the evolution of undermassive, overmassive, and median BHs and their hosts onto both the $z = 0.05$ $M_{BH}-M_{star}$ relation and $M_{acc}-M_{star}$ relation. The black line indicates the SS13 locally observed relation, where the dashed portion indicates a linear extrapolation. Regardless of
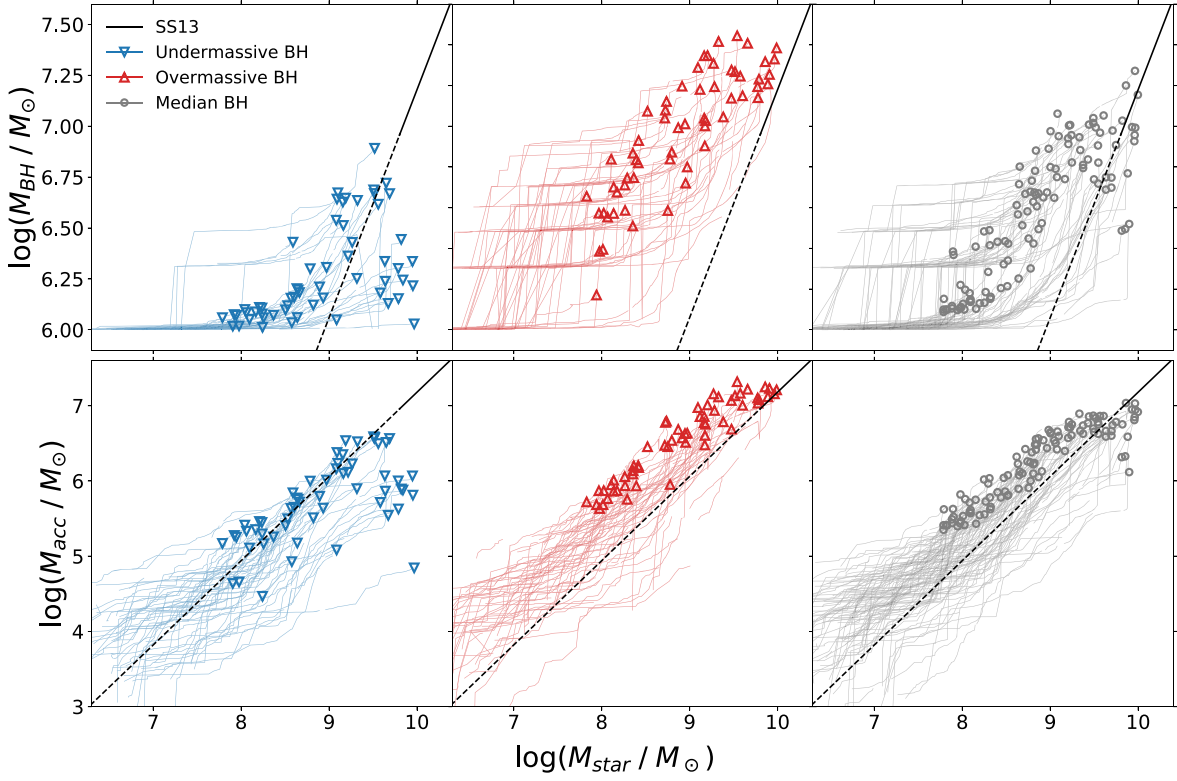
Figure 4. Evolution of BHs and their host galaxies, separated by undermassive (left), overmassive (center), and median BHs (right). The black line indicates the Schramm & Silverman (2013) relation, where the dashed portion indicates the extrapolated relation. We plot both the growth of total BH mass and total BH accretion. Top: evolution onto the $z = 0.05$ $M_{\rm BH}-M_{\rm star}$ relation. Bottom: evolution onto the $z = 0.05$ $M_{\rm acc}-M_{\rm star}$ relation. Hosts of undermassive BHs tend to build up their stars more rapidly than their BHs, evolving onto the $z = 0.05$ relation by growing stars first and then BHs later. Hosts of overmassive BHs tend to build up their BHs rapidly before growing in stellar mass onto the $z = 0.05$ relation. Median BHs tend to grow closer along the extrapolated SS13 relation.

how we frame BH growth, we find fundamental differences in growth histories between undermassive and overmassive BH hosts. Undermassive BHs tend to evolve onto the $z = 0.05$ relation by building up $M_{\rm BH}$ only after the host has built up its stars. On the other hand, overmassive BH hosts tend to either grow their BHs before their stellar mass or grow both in tandem. The differences in $M_{\rm BH}-M_{\rm star}$ evolution strongly suggest that overmassive and undermassive BH hosts may build up their stars and dark matter in fundamentally different ways.

3.3. Galaxy and Halo Growth

With the growth histories of the BHs in hand, we now study the environments in which they formed and reside. We trace the structural evolution of stars and dark matter in the BH hosts across cosmic time. In the following analysis we consider the 197 isolated dwarf galaxies in ROMULUS25 that do not host any BHs alongside the 205 that do host BHs, in order to better understand the role of BHs in structural evolution.

Munshi et al. (2013) identify a systematic overestimate in dark-matter-only (DMO) simulation halo masses when compared to simulations that include baryon physics and outflows. When comparing with results from DMO simulations, we adjust halo masses such that $M_{\rm 200,sim} = 0.8M_{\rm 200,DMO}$ for halos with masses $M_{200} = 10^8-10^{12}M_{\odot}$.

#### 3.3.1. Stellar Mass–Halo Mass Relation

Figure 5 shows the $z = 0.05$ stellar mass–halo mass (SMHM) relation for all isolated ROMULUS25 galaxies, with masses adjusted with corrections from Munshi et al. (2013).

Points are colored by whether the hosted BH is overmassive, undermassive, or median, or if the galaxy does not host a BH. A similar figure of the SMHM relation in ROMULUS25 for all central halos can be found in Tremmel et al. (2017). We mark the $M_{\rm star} = 10^{10}M_{\odot}$ dwarf galaxy boundary and limit the axes to focus on low-mass galaxies. We include abundance matching estimates from Moster et al. (2013) and Kravtsov et al. (2018) for reference. Above $M_{200} > 10^{11}M_{\odot}$, overmassive BHs tend to be found in halos with lower stellar masses than expected for their halo mass. Undermassive BHs instead tend to be found in halos with higher stellar masses than expected for their halo mass. Undermassive and median BH hosts in particular tend to sit along or above abundance matching estimates of the SMHM relation. Galaxies without BHs follow a similar relation to undermassive BH hosts, and above $M_{200} > 10^{11}M_{\odot}$ they sit at higher $M_{\rm star}$ than overmassive BH hosts at a given halo mass.

To better quantify the connection between scatter in $M_{\rm acc}$ and scatter in $M_{\rm star}$, we define the residual quantities $\Delta \log M_{\rm acc}$ and $\Delta \log M_{\rm star}$. We fit a smoothing spline to the median SMHM relation for all isolated ROMULUS25 galaxies and then calculate $\Delta \log M_{\rm star}$ as the residual from the median $\log M_{\rm star}$ for a given halo mass. We similarly fit a spline to the median $M_{\rm BH}-M_{\rm star}$ relation and use the previous fit to find the expected $M_{\rm acc}$ for a given halo mass. We then calculate $\Delta \log M_{\rm acc}$ as the residual from the median. Figure 6 shows $\Delta \log M_{\rm acc}$ versus $\Delta \log M_{\rm star}$, split between galaxies with stellar mass $10^8M_{\odot} < M_{\rm star} < 10^9M_{\odot}$ and $10^9M_{\odot} < M_{\rm star} < 10^{10}M_{\odot}$. We split our sample in this way to better isolate resolution effects at the lowest masses. We distinguish
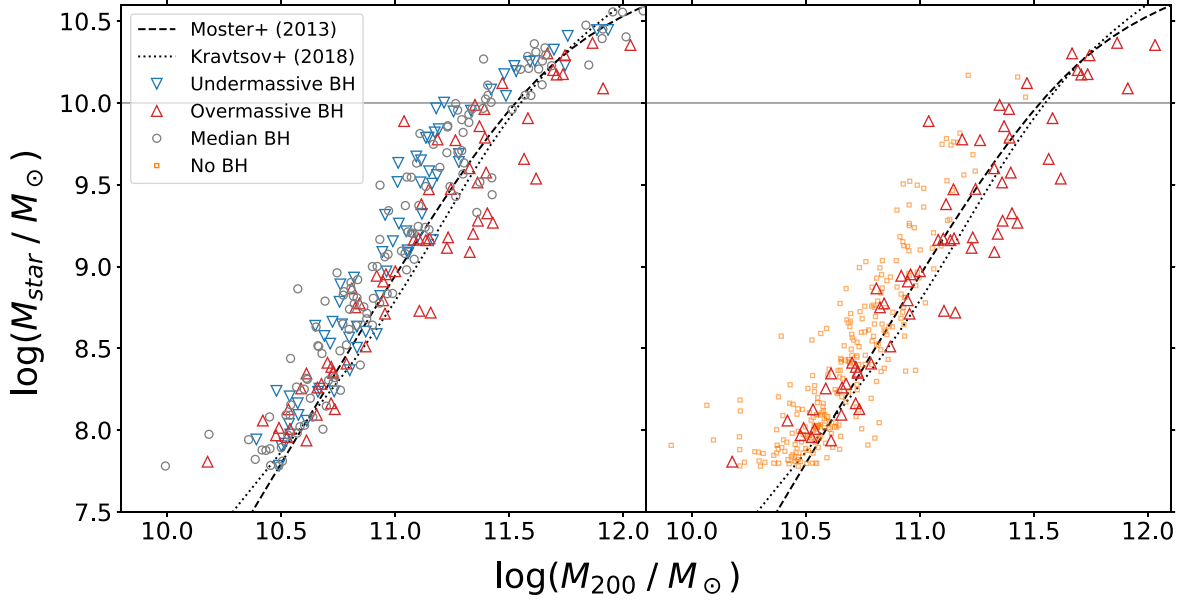
Figure 5. The $z = 0.05$ stellar mass vs. halo mass relation for isolated ROMULUS25 galaxies. Stellar and halo masses are adjusted using corrections from Munshi et al. (2013). We compare with abundance matching estimates from Moster et al. (2013) (black dashed) and Kravtsov et al. (2018) (black dotted). We limit the axes to focus on dwarf galaxy masses and mark the $M_{\rm star} = 10^{10} M_\odot$ dwarf galaxy boundary (gray solid). Left: comparison of overmassive (red triangles), undermassive (blue inverted triangles), and median (gray circles) BH hosts. Above $M_{200} > 10^{11} M_\odot$, overmassive BH hosts tend to sit at lower stellar masses than expected for the corresponding halo mass. Undermassive and median BHs tend to sit along or slightly above abundance matching estimates of the SMHM relation. Right: comparison of overmassive BH hosts with isolated galaxies that do not host a BH (orange squares). Galaxies without BHs exhibit a similar relation to galaxies hosting undermassive BHs, sitting along or slightly above both abundance matching estimates and overmassive BHs hosts.
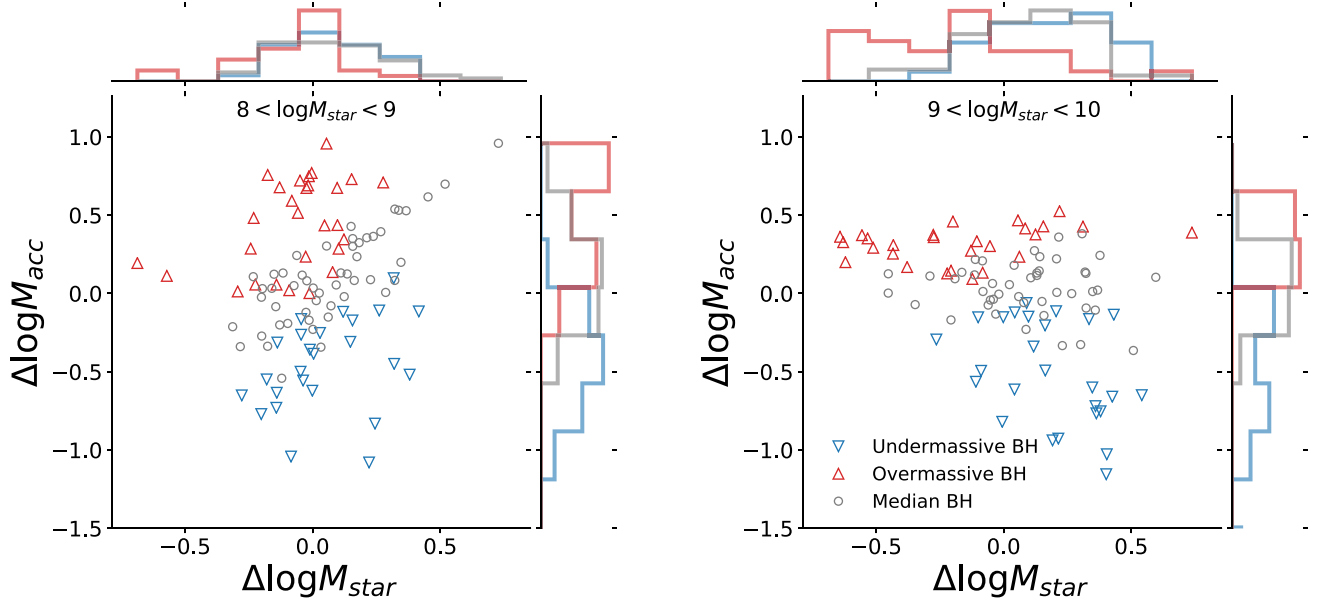

Figure 6. Residual quantities $\Delta \log M_{\rm acc}$ vs. $\Delta \log M_{\rm star}$ (see text for definitions), split by galaxies with stellar mass $10^8 M_\odot < M_{\rm star} < 10^9 M_\odot$ (left) and $10^9 M_\odot < M_{\rm star} < 10^{10} M_\odot$ (right). Points are colored by whether the hosted BH is overmassive (red triangles), undermassive (blue inverted triangles), or median (gray circles). We also include normalized marginal histograms for each classification. Left: hosts of undermassive and overmassive BHs show identical distributions of $\Delta \log M_{\rm star}$. Right: galaxies with higher $\Delta \log M_{\rm acc}$ tend to be found at lower $\Delta \log M_{\rm star}$, and vice versa. Overmassive BH hosts tend to have the lowest $\Delta \log M_{\rm star}$.

between hosts of overmassive, undermassive, and median BHs. Positive/negative $\Delta \log M_{\rm acc}$ roughly correspond with overmassive/undermassive BHs.

We find that overmassive BHs tend to be found in halos with fewer stars than expected from the median, while undermassive BHs are found in halos with more stars than expected. For galaxies with $10^9 M_\odot < M_{\rm star} < 10^{10} M_\odot$,

overmassive BHs tend to be found at lower $\Delta \log M_{\rm star}$ and higher $\Delta \log M_{\rm acc}$ than their undermassive counterparts. Galaxies with $10^8 M_\odot < M_{\rm star} < 10^9 M_\odot$ show little difference in $\Delta \log M_{\rm star}$ between overmassive and undermassive BHs. This result implies that BH accretion, and hence feedback, may suppress star formation in isolated galaxies between $10^9 M_\odot < M_{\rm star} < 10^{10} M_\odot$.
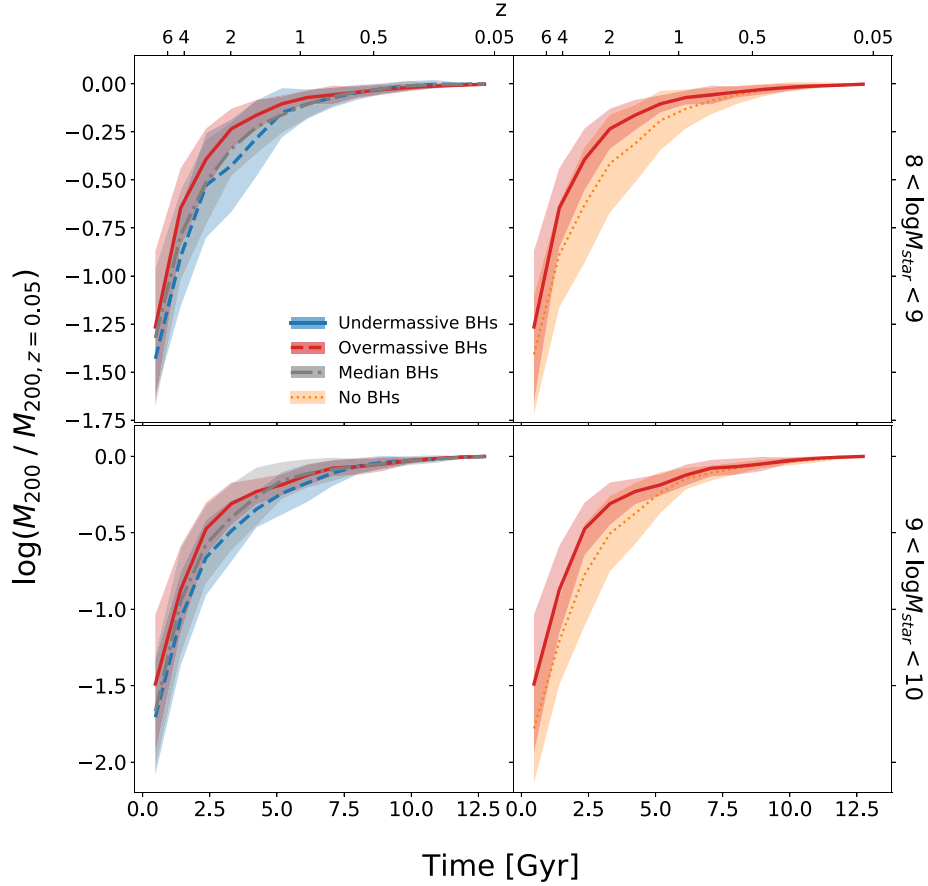
Figure 7. Median time evolution of halo mass of the main halo progenitor, scaled by the final $z = 0.05$ halo mass. The left panels compare the halo mass evolution of hosts of undermassive (blue dashed), overmassive (red solid), and median (gray dashed–dotted) BHs. The right panels compare the halo mass evolution of isolated galaxies without BHs (orange dotted) to the evolution of overmassive BH hosts. The top panels show galaxies with stellar mass $8M_\odot < M_{star} < 9M_\odot$, while the bottom panels show galaxies with stellar mass $9M_\odot < M_{star} < 10M_\odot$. Shaded regions indicate 1σ scatter in evolutionary tracks. Regardless of final stellar mass, hosts of overmassive BHs tend to build up their halo mass before hosts of undermassive BHs, as well as before galaxies without BHs. Undermassive BHs show a similar delay to galaxies without BHs in growing their halos.

3.3.2. Structural Evolution

We now turn to the impact of BHs on the structural evolution of dark matter and stars. We find that the undermassive/overmassive nature of a BH is directly tied to the structural evolution of its host. Figure 7 shows the evolution of M_{200} of the main halo progenitor, scaled by M_{200} at $z = 0.05$, distinguishing between undermassive, overmassive, and median BH hosts. We also include a comparison between galaxies hosting overmassive BHs and galaxies without BHs. We distinguish between galaxies with $z = 0.05$ stellar mass $10^8 M_\odot < M_{star} < 10^9 M_\odot$ and $10^9 M_\odot < M_{star} < 10^{10} M_\odot$. Overmassive BH hosts tend to build up their halos earlier than both hosts of undermassive BHs and galaxies without BHs. The delay in halo growth is most pronounced in dwarf galaxies above $M_{star} > 10^9 M_\odot$ at $z = 0.05$.

Figure 8 similarly shows the median cumulative star formation history for each class of BH hosts. Overmassive BH hosts build up their stellar mass much more rapidly than both hosts of undermassive BHs and galaxies without BHs. As with halo mass, the differences in stellar mass evolution are most pronounced in dwarf galaxies above $M_{star} > 10^9 M_\odot$ at $z = 0.05$.

Further analysis shows that the formation of overmassive/undermassive BHs can likely be attributed to differences in

halo assembly times. We fit each halo density profile with a flexible five-parameter model (Dekel et al. 2017):

$$\rho(r) = \frac{\rho_c}{x^\alpha (1 + x^{1/\beta})^{\beta(\gamma-\alpha)}}, \qquad (5)$$

where α and γ are, respectively, the inner and outer profile slopes, β is the intermediate shape parameter, and the radius is scaled by the scale radius, R_s, which is related to the halo concentration, c,

$$x = \frac{r}{R_s}, \qquad c = \frac{R_{200}}{R_s}. \qquad (6)$$

Figure 9 shows the evolution of halo concentration over time. Overmassive BH hosts have higher halo concentrations than their undermassive counterparts (see Macciò et al. 2008; Zhao et al. 2009, and references therein), as well as halos without BHs. A two-sample, two-sided Kolmogorov–Smirnov (K-S) test on overmassive versus undermassive BH host concentrations yields a K-S statistic $D_{n,m} = 0.29$ and allows us to reject the null hypothesis at the 0.02 level that the halos are drawn from the same distribution of concentrations. Similarly, a K-S test on overmassive BH hosts versus halos without BHs yields a K-S statistic $D_{n,m} = 0.45$ and allows us to reject the null hypothesis at the 8×10^{-8} level.
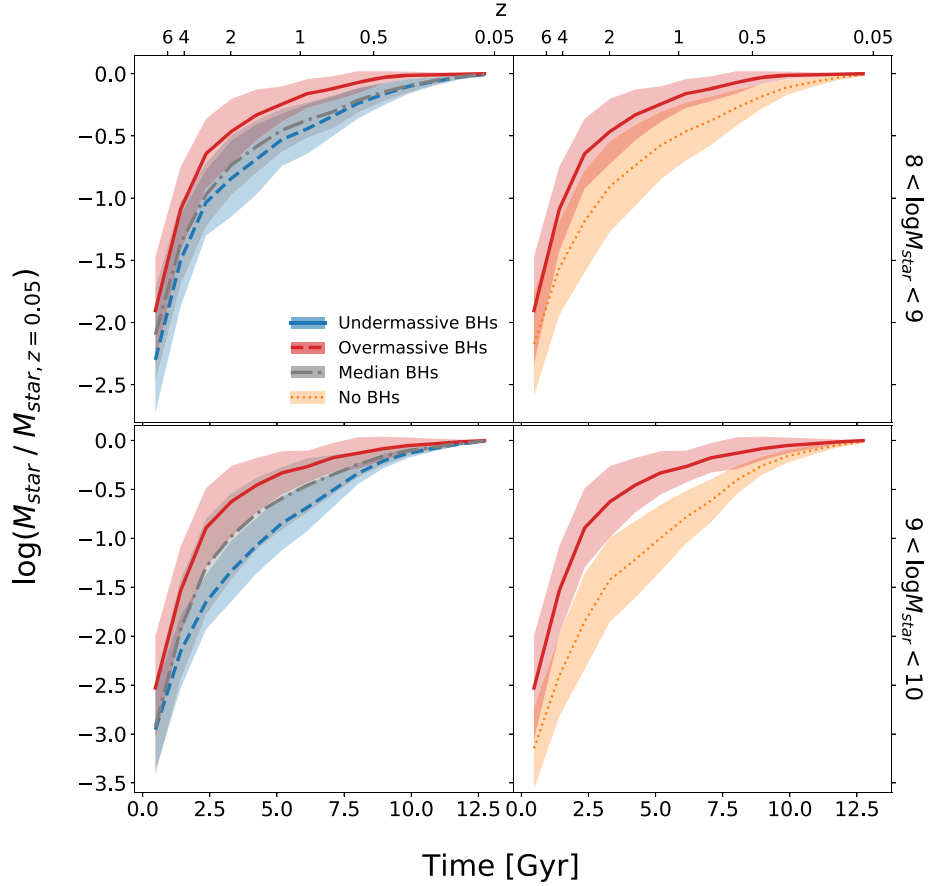
Figure 8. Median time evolution of stellar mass, scaled by the final $z = 0.05$ stellar mass. The left panels compare the stellar mass evolution of hosts of undermassive (blue dashed), overmassive (red solid), and median (gray dashed–dotted) BHs. The right panels compare the stellar mass evolution of isolated galaxies without BHs (orange dotted) to the evolution of overmassive BH hosts. The top panels show galaxies with stellar mass $10^8 M_\odot < M_{star} < 10^9 M_\odot$, while the bottom panels show galaxies with stellar mass $10^9 M_\odot < M_{star} < 10^{10} M_\odot$. Shaded regions indicate 1σ scatter in evolutionary tracks. Hosts of overmassive BHs build up their stellar mass a few gigayears before hosts of undermassive BHs, as well as before galaxies without BHs. The differences in growth histories are most apparent in galaxies with final stellar masses $10^9 M_\odot < M_{star} < 10^{10} M_\odot$. Undermassive BHs show a similar delay to galaxies without BHs in growing their stellar mass.

The buildup of stars prior to BH growth, the lack of BH mergers in undermassive BH hosts, and the lower halo concentrations all suggest that undermassive BHs initially formed in environments with a lower abundance of cold gas than is necessary to seed multiple BHs. In contrast, overmassive BHs were likely initially seeded in environments with an abundance of cold gas, where BHs had a higher likelihood to merge and accrete efficiently.

There is strong evidence that the central regions of massive galaxies are most affected by the presence of a central BH (Cheung et al. 2012; Barro et al. 2017; Choi et al. 2018). We trace the evolution of stars within the central regions of the host galaxy and search for a connection to the central BH.

We define the stellar mass surface density within the stellar half-light radius, r_e:

$$\Sigma_e = \frac{M_{star}(<r_e)}{\pi r_e^2}, \qquad (7)$$

where we calculate r_e by fitting a Sérsic profile to the projected face-on V-band surface brightness profile, with a surface brightness cutoff of 32 mag arcsec^{-2} (Abraham & van Dokkum 2014).

Cheung et al. (2012) find that stellar density within the central 1 kpc, Σ_1, robustly follows quenching in local galaxies

above $M_{star} \gtrsim 10^8 M_\odot$. Chen et al. (2019) build a schematic model that finds that galaxies begin to rapidly quench once they evolve over a boundary in $\Sigma_1 - M_{star}$ space. Many ROMU-LUS25 dwarf galaxies fall below $r_e < 1$ kpc at early times; hence, we use r_e to consistently define a central region across time. Both Franx et al. (2008) and Barro et al. (2013) find a strong relationship between Σ_e and both the star formation rate (SFR) and total stellar mass out to $z \sim 3.5$. Hence, tracing the evolution of Σ_e while distinguishing between hosts of overmassive and undermassive BHs can give insight into the effects of BH growth on central star formation.

Figure 10 shows the evolution of Σ_e across time for galaxies with undermassive, overmassive, and median BHs, as well as for galaxies without BHs. We distinguish between galaxies with $z = 0.05$ stellar mass $10^8 M_\odot < M_{star} < 10^9 M_\odot$ and $10^9 M_\odot < M_{star} < 10^{10} M_\odot$. Similar to the buildup of total stellar mass, overmassive BH hosts build up their central stellar density more rapidly than both undermassive BH hosts and galaxies without BHs. However, above $M_{star} > 10^9 M_\odot$, overmassive BH hosts show suppression of Σ_e growth starting at redshift $z \sim 2$. By $z \sim 0.5$, many hosts of undermassive BHs and galaxies without BHs reach 0.5 dex higher Σ_e than hosts of overmassive BHs. Hosts of undermassive BHs and galaxies without BHs may instead flatten in Σ_e at late times, around $z \sim 0.1$. We confirm that these results would remain
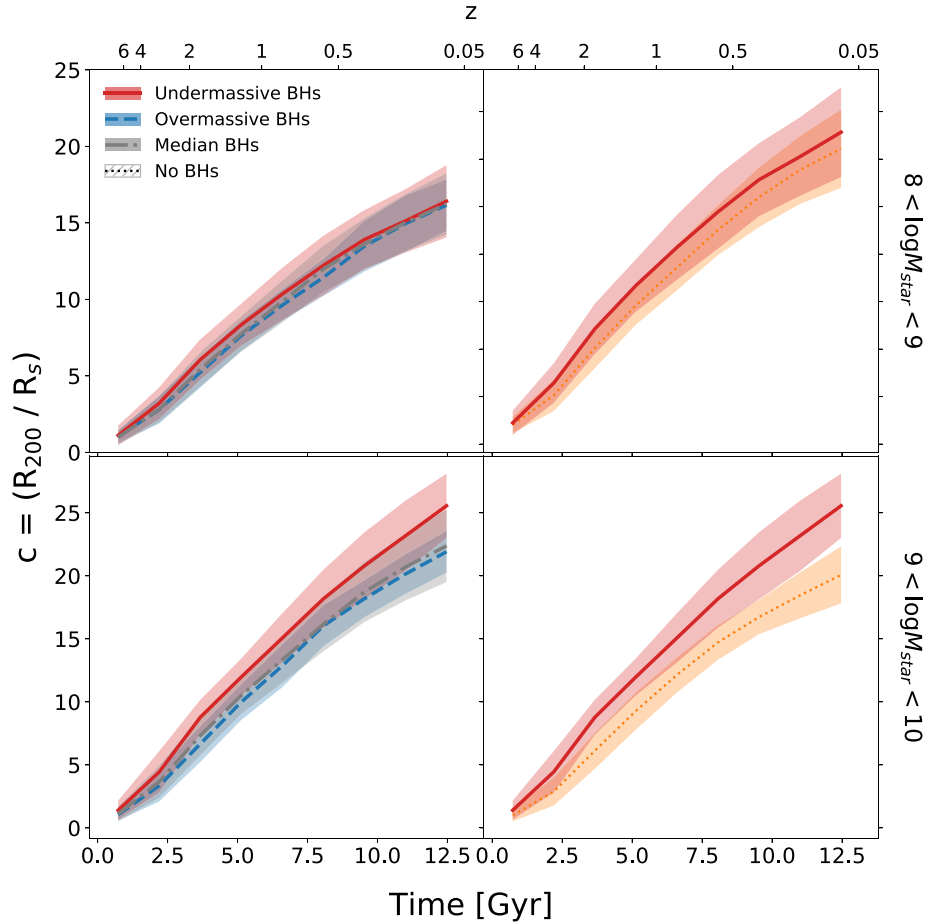
Figure 9. Median time evolution of halo concentration of the main halo progenitor. Ordering of panels and legend are the same as in Figure 7. For halos with final stellar mass $9 < \log M_{star} < 10$, those that form overmassive BHs are more concentrated than their undermassive counterparts and are more concentrated than halos without BHs by $z = 0.05$. Halos with final stellar mass $8 < \log M_{star} < 9$ show little variation in halo concentrations across time.

qualitatively the same were we to use surface densities calculated within the central 1 kpc rather than r_e.

In short, overmassive BHs were first seeded in early-forming halos, building up their dark matter and stars rapidly in tandem with growth of the BH. Despite having higher halo concentrations, overmassive BH hosts have similar or lower central stellar density than their undermassive counterparts by late times, indicating a measure of star formation suppression within the central regions. Undermassive BH hosts instead follow nearly identical evolutionary tracks to galaxies without BHs, growing dark matter and stars later and exhibiting high central stellar densities at late times. Dickey et al. (2019) find a similar relationship in isolated galaxies with stellar mass $10^9 M_\odot < M_{star} < 10^{9.5} M_\odot$, where strong signatures of AGNs correlate with an older stellar population in the host galaxy. Li et al. (2020) similarly find that overmassive BH hosts form earlier and have lower present-day SFRs.

Choi et al. (2018) find similar evolution of Σ_e in zoom-in simulations of galaxies with $M_{star} > 10^{10.9} M_\odot$ run with and without AGN feedback. They find that galaxies with AGN feedback build up Σ_e until $z \sim 2$, after which Σ_e turns over and begins to decrease. The stellar cores become diffuse primarily through AGN-driven stellar mass loss and gas mass loss "puffing up" the central region. They find that the turnover in Σ_e is concurrent with quenching of star formation. Galaxies run without AGN feedback indefinitely increase their central stellar

densities and do not experience the same level of quenching. Both Guo et al. (2013) and Barro et al. (2017) similarly observe that stellar cores diffuse over time in CANDELS GOODS-S galaxies with stellar masses $10^9 M_\odot < M_{star} < 10^{11.5} M_\odot$.

Stagnation in central stellar density can come about in a few ways. Stellar evolution can eject mass from stars and return it to gas in the ISM (van Dokkum et al. 2014). Mass loss through stellar outflows directly competes with new star formation promoted by the increased gas mass (Kennicutt et al. 1994). As a result, Choi et al. (2018) find this effect to contribute little to central stellar density suppression.

Compaction events may occur through strongly dissipational, gas-rich mergers driving stars and gas toward the galaxy center. Conversely, gas-poor mergers can reduce the core stellar density by driving rapid size growth with little growth in mass (Hopkins et al. 2008; Nipoti et al. 2009; Covington et al. 2011; Oser et al. 2012; Hilz et al. 2013; Porter et al. 2014). Overmassive BH hosts in ROMULUS25 are often found to have up to 4 orders of magnitude lower gas fractions relative to galaxies without BHs (see Section 3.4.2) and hence may be subject to stellar diffusion through gas-poor mergers, though we find no evidence of major mergers driving rapid changes in stellar or gas profiles of overmassive or median BH hosts.

There are other physical processes that have been commonly found to reduce central stellar density but are unresolved in ROMULUS25. Binary BH systems may be capable of clearing
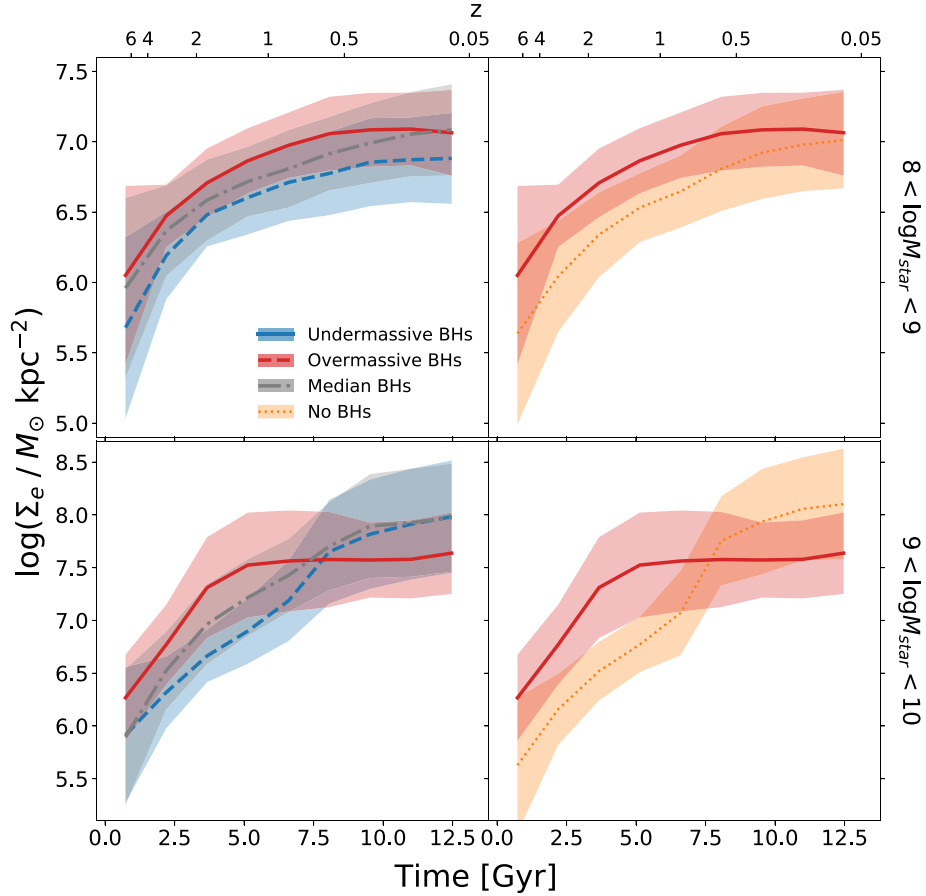
Figure 10. Median time evolution of central stellar mass surface density (see text for definition of Σ_e). The left panels compare the evolution of hosts of undermassive (blue dashed), overmassive (red solid), and median (gray dashed–dotted) BHs. The right panels compare the evolution of isolated galaxies without BHs (orange dotted) to the evolution of overmassive BH hosts. The top panels show galaxies with stellar mass $10^8 M_\odot < M_{star} < 10^9 M_\odot$, while the bottom panels show galaxies with stellar mass $10^9 M_\odot < M_{star} < 10^{10} M_\odot$. Shaded regions indicate 1σ scatter in evolutionary tracks. Overmassive BH hosts grow stellar mass in their central regions more quickly than hosts of undermassive BHs, as well as more quickly than galaxies without BHs. Between $10^8 M_\odot < M_{star} < 10^9 M_\odot$, galaxies reach the same central densities by $z = 0.05$. Between $10^9 M_\odot < M_{star} < 10^{10} M_\odot$, overmassive BH hosts stop growing in Σ_e around $z \sim 1$. Undermassive BH hosts and galaxies without BHs in this mass range continue growing, reaching higher Σ_e at late times than overmassive BH hosts.

out galaxy cores (Milosavljević & Merritt 2001; Kormendy et al. 2009), but BH scouring occurs on scales below the spatial resolution limit of ROMULUS25 (Rantala et al. 2017, 2018). Mass loss and heating driven by outflows and SNe may reduce the gravitational potential and in turn allow for outward stellar migration (Fan et al. 2008; Choi et al. 2018), but ROMU-LUS25 does not resolve these effects on the central potential.

Finally, heating and mass loss driven by outflows and SNe can in turn drive gas outward, restrict gas cooling, and hence suppress star formation (Somerville & Davé 2015). Below we show that the differences in structural evolution between ROMULUS25 galaxies with overmassive BHs and other galaxies are likely due to this BH feedback.

3.4. Impact of BHs on Stars and Gas

3.4.1. Energy Injection by BHs

We find that median and overmassive BHs are capable of injecting more energy than SNe into the surrounding gas of their hosts. We calculate total energy injection via BHs and SNe by first integrating their energy outputs across cosmic time. A set fraction of the energy output is injected into the surrounding ISM (see Section 2.1). Figure 11 shows the ratio of energy injected by BHs to SNe versus the host stellar mass.

Many overmassive and median BHs are capable of injecting substantially more energy than SNe. On the other hand, undermassive BH hosts are all dominated by energy injection by SNe. At all stellar masses, overmassive BHs hosts are injected with two to three more combined BH + SN energy than undermassive BH hosts.

A higher E_{BH}/E_{SN} suggests that outflows from BHs may more efficiently heat and drive gas than SNe outflows. It is important to note that while BHs produce and inject copious amounts of energy, it is ultimately the feedback prescription that determines the effect on the host. Feedback models that inject kinetic energy typically drive winds at higher velocities than those that inject purely thermal energy (Choi et al. 2018).

3.4.2. Cold Gas Depletion

Next, we turn to the relationship between BHs and the amount of cold gas in the host galaxy. Figure 12 shows the H I gas mass versus stellar mass relation for isolated dwarf galaxies. We compare with observations from Bradford et al. (2018) and Catinella et al. (2018). Bradford et al. combine a new set of 21 cm observations with the H I-selected ALFALFA survey (Haynes et al. 2011) to analyze gas depletion in local galaxies ($0.002 < z < 0.055$) with stellar mass $10^7 M_\odot < M_{star} < 10^{9.5} M_\odot$. Catinella et al. measure H I
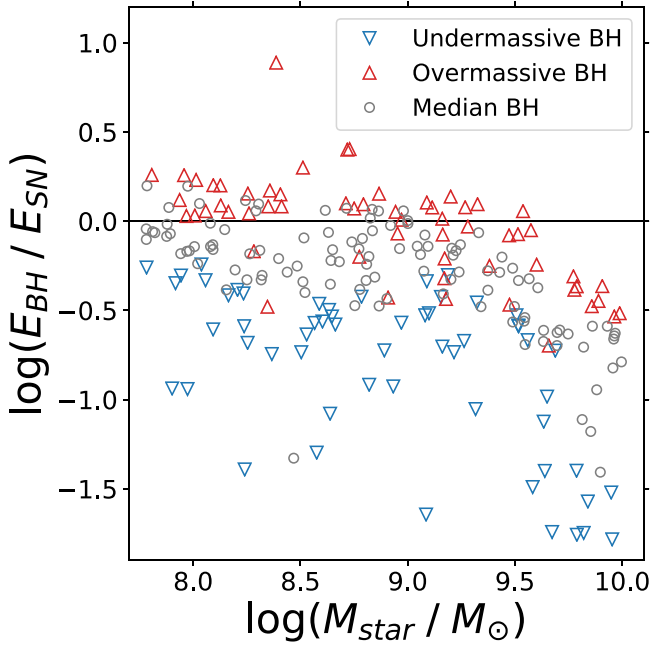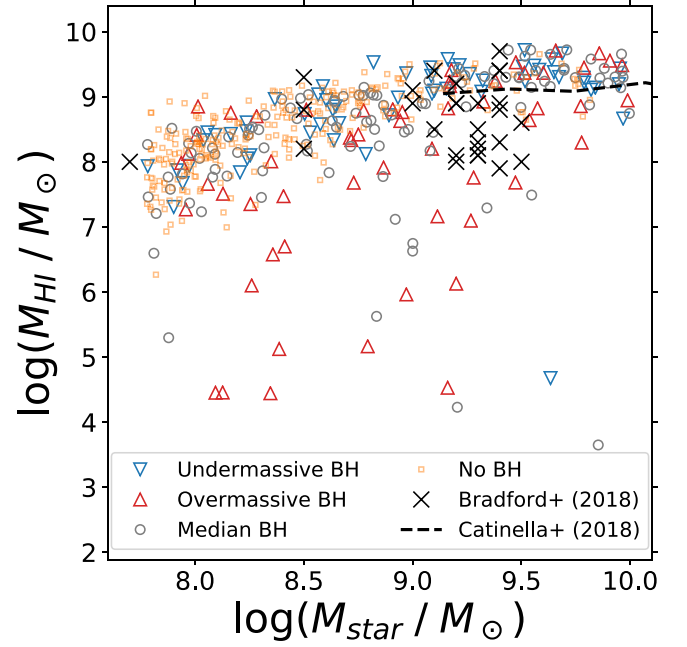
Figure 11. Ratio of the total energy injected by BHs to the total energy injected by SNe over cosmic time vs. the stellar mass of the host galaxy at $z = 0.05$. Galaxies are colored by whether they host an overmassive (red triangles), undermassive (blue inverted triangles), or median (gray circles) BH. We mark the $E_{BH} = E_{SN}$ boundary (black line). Undermassive BH hosts are all dominated by energy injection from SNe. Regardless of host stellar mass, overmassive and median BHs are often capable of injecting more energy than SNe.

Figure 12. H I gas mass vs. stellar mass for hosts of overmassive (red triangles), undermassive (blue inverted triangles), and median (gray circles) BHs. Galaxies without BHs are also shown (orange squares). We compare with observed $M_{H I}$–M_{star} relations from Bradford et al. (2018) (black crosses) and Catinella et al. (2018) (dashed black). Undermassive BH hosts and galaxies without BHs agree well with the observations. Overmassive BH hosts tend to have significantly less H I gas than other galaxies at the same stellar mass.

content of local $(0.01 < z < 0.05)$ stellar-mass-selected xGASS galaxies, with stellar masses $10^9 M_\odot < M_{star} < 10^{11.5} M_\odot$.

Hosts of undermassive BHs and galaxies without BHs follow the Catinella et al. relation at the high-mass end and are consistent with nondepleted galaxies from Bradford et al. across all stellar masses. Hosts of undermassive BHs and galaxies without BHs show little indication of significant cold gas depletion. On the other hand, many overmassive and median BH hosts exhibit lower $M_{H I}$ than expected for their stellar mass, indicating a high degree of cold gas depletion. Although ALFALFA is most sensitive to H I above $M_{H I} \gtrsim 10^7 M_\odot$, it is worth noting that the extreme levels of cold gas depletion seen in overmassive BH hosts are often orders of magnitude below what is seen in either observational comparison sample. Bradford et al. similarly find that isolated galaxies with stellar mass $10^{9.2} M_\odot < M_{star} < 10^{9.5} M_\odot$ with strong signatures of AGNs tend to show a higher degree of gas depletion than similar galaxies with weaker AGN signatures, though they find that this effect does not extend to more massive galaxies. Bradford et al. do not rule out the ejection and heating of cold gas by unusually bursty and compact star formation activity.

3.4.3. Star Formation Quenching

Tremmel et al. (2019) fit the ROMULUS25 star formation main sequence by calculating median values of the SFR within 0.1 dex bins of stellar mass between $10^8 M_\odot < M_{star} < 10^{10} M_\odot$, for galaxies considered relatively isolated by the same criteria we use in this work. They find a best fit of $\log(\text{SFR}) = 1.206 \times \log(M_{star}) - 11.7$ at $z = 0$. We define galaxies whose SFR falls a factor of 10 below the main sequence to have

quenched star formation. We calculate SFRs averaged over the previous 250 Myr.

Figure 13 shows the $z = 0.05$ star formation main sequence for ROMULUS25 dwarf galaxies. We distinguish between hosts of overmassive, undermassive, and median BHs, as well as isolated galaxies without BHs. Quenched galaxies are marked with filled points. We mark the Tremmel et al. (2019) relation with a solid line.

Quenching tends to occur in isolated dwarf galaxies that host overmassive or median BHs. We find 12 quenched dwarf galaxies, 7 of which host a BH. Above $M_{star} \gtrsim 10^{8.6} M_\odot$, quenching only occurs in dwarf galaxies that host BHs. Quenched galaxies that host a BH tend to host overmassive BHs, regardless of host stellar mass.

To help identify the source of quenching as internal or external, we track the interaction history of each galaxy of interest and estimate the tidal effects of close encounters. Following Karachentsev & Makarov (1999), we calculate tidal indices, Θ, such that

$$\Theta = \max\{\log(M_k/D_k^3)\} - 11.75, \qquad (8)$$

$$k = 1, 2, ..., N, \qquad (9)$$

where M and D are the masses and 3D separations, respectively, of the kth closest halo. Negative values of Θ indicate no tidal disturbance of the main halo by nearby halos, while high positive values (we arbitrarily choose $\Theta > 5$) indicate significant tidal disturbance.

Analyzing the encounter history of our quenched galaxies, there is one undermassive BH host that is particularly close to the quenched boundary, and further analysis reveals that it was
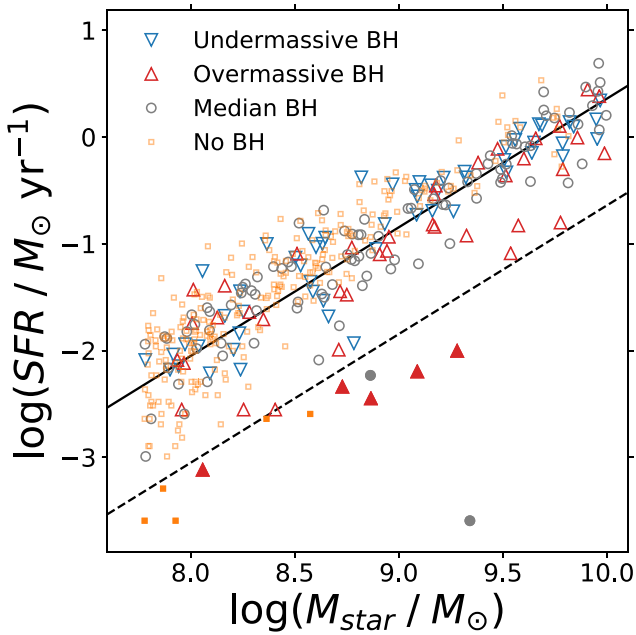
Figure 13. SFR vs. stellar mass for hosts of overmassive (red triangles), undermassive (blue inverted triangles), and median (gray circles) BHs. Galaxies without BHs are also shown (orange squares). We plot the $z = 0$ ROMULUS25 main sequence as calculated by Tremmel et al. (2019) (black solid) and the quenched boundary 1 dex below the main sequence (black dashed). Filled points indicate galaxies we consider quenched (see text for details). The majority of quenched galaxies with BHs host overmassive BHs. Galaxies without BHs can be quenched, but they are all found at lower stellar masses, $M_{star} < 10^9 M_{\odot}$.

stripped of H I gas and quenched immediately following tidal disturbance by a more massive halo. Similarly, the two quenched median BH hosts both show evidence of such encounters followed by H I depletion and quenching. Of the five quenched overmassive BHs, two exhibit high tidal indices from encounters with massive halos. Thus, quenching can occur in galaxies below $M_{star} < 10^{8.6} M_{\odot}$ even if they do not host a BH, though all but one show clear evidence of past encounters with a more massive galaxy and a subsequent drop in star formation.

As discussed in Tremmel et al. (2019), our definition of quenched is different from some observations, such as Wetzel et al. (2012), who adopt a flat threshold in specific SFR of 10^{-11} yr^{-1}. Regardless, our results change little when we instead use a flat specific SFR threshold of 10^{-11} yr^{-1}.

Although ROMULUS25 uses a purely thermal feedback model, simulations have found success in using feedback models that incorporate both thermal feedback and mechanical feedback that efficiently drives high-velocity winds. Choi et al. (2015) find that the inclusion of mechanical feedback more efficiently suppresses late-time star formation and produces AGN luminosities in line with observations. Choi et al. (2016) find that mixed thermal and mechanical AGN feedback models yield reasonable results for ex situ and in situ star formation and realistic gas and stellar structural properties. Weinberger et al. (2017) find that dual-mode AGN feedback for weakly/ highly accreting BHs yields realistic star formation suppression, gas fractions, BH growth, and thermodynamic profiles.

Our findings are in line with results from Ricarte et al. (2019), who find that isolated ROMULUS25 galaxies with

$M_{star} > 10^{9.5} M_{\odot}$ show signs of coevolution with their central BH. Ricarte et al. find that the BH accretion rate follows the SFR in star-forming galaxies, regardless of redshift, stellar mass, or large-scale environment. Further, they find that such BHs grow in tandem with their host galaxies, eventually being confined to a line of constant M_{BH}/M_{star}. They suggest that self-regulation of BH growth through feedback is a possible driver of coevolution seen in isolated ROMULUS25 galaxies.

3.5. Caveats

Our analysis of the role of BHs in dwarf galaxy evolution has a few caveats. Although we find correlations between BH properties and properties of the host galaxy, the precise effect of BH activity on dwarf galaxy evolution is unclear. We have not directly traced the effects of BHs on the surrounding environment (e.g., tracing outflows, tracking heating, turning off BH physics, and rerunning the simulation), and hence we cannot say for certain how BHs may drive changes in their hosts within ROMULUS25. Further, observations from Mezcua et al. (2019) find that dwarf galaxies can host powerful jets whose mechanical feedback may strongly impact the host star formation history, an effect that is not accounted for in ROMULUS25. We find no evidence of starbursts in compact galaxies (Diamond-Stanic et al. 2012) as the dominant mechanism driving trends in star formation suppression, though the spatial resolution of ROMULUS25 likely restricts especially compact galaxies from forming. It appears that BH feedback plays a larger role than often thought within dwarf galaxies (Martín-Navarro & Mezcua 2018), and it is likely that both stellar feedback and BH feedback together drive suppression of central stellar density and overall star formation in ROMULUS25 dwarf galaxies. Future work will further analyze the role of AGNs in the evolution of dwarf galaxies, in particular how BH activity relates to suppression of star formation.

As seen in Equation (3), accretion onto BHs is sensitive to the BH mass. This is particularly important for two reasons: (1) some BHs in ROMULUS25 may unphysically merge immediately after seeding, and (2) the seed mass is likely too high in the lowest-mass galaxies. Some BHs effectively form at higher masses than the seed mass owing to seeding of multiple, clustered BHs and subsequent rapid merging. Bellovary et al. (2019) find a similar phenomenon in zoom-in simulations of dwarf galaxies. Bellovary et al. define "overmerging" to occur if either of the merging BHs were seeded <100 Myr prior to the merger event. They suggest that this time frame is long enough for BH feedback from existing BHs to suppress future BH formation. We find that approximately 35% of overmassive BHs and 15% of median BHs have experienced an over-merging event. Since BHs that undergo BH mergers have a subsequently higher accretion rate, such overmerging may unphysically contribute to the BH mass. However, we find that overmerging does not guarantee that a BH will become overmassive or grow to high M_{BH}.

Finally, current observations of BHs in dwarf galaxies indicate that BHs may have masses lower than the BH seed mass used in this work (Baldassare et al. 2015; Reines & Volonteri 2015; Nguyen et al. 2017, 2018, 2019; Schutte et al. 2019). Observed BH masses in $M_{star} \sim 10^9$ galaxies are typically a few $\times 10^5 M_{\odot}$ but can reach as low as $6.8 \times 10^3 M_{\odot}$ (Nguyen et al. 2019). Mezcua et al. (2018) combine Chandra data of $z \lesssim 2.4$ dwarf galaxies with the

$M_{BH}-M_{star}$ relation from Reines & Volonteri (2015) and calculate BH masses consistent with the undermassive but not the overmassive BH masses in this work. In particular, overmassive BHs in ROMULUS25 may be unrealistically massive and accrete too much, causing us to overestimate their ability to drive galaxy-scale changes through feedback. Moving to higher-resolution simulations in the future may give a more clear understanding of both how BHs grow within dwarf galaxies and how dwarf galaxies may have their star formation suppressed by the BH.

4. Summary

We explore the connections between BH growth and dwarf galaxy evolution within the ROMULUS25 cosmological simulation. We investigate the source of scatter in the $M_{BH}-M_{star}$ relation and classify BHs as overmassive, undermassive, or median for their host M_{star}. Using these classifications, we follow the primary growth modes for both BHs and their hosts. We can summarize our results as follows:

1. ROMULUS25 forms massive BHs at early times in well-resolved dwarf galaxies ($10^8 M_\odot < M_{star} < 10^{10} M_\odot$) that are consistent with observed BH scaling relations above $M_{star} \gtrsim 10^{8.5} M_\odot$. The $M_{BH}-M_{star}$ relation shows a high degree of scatter in galaxies below $M_{star} < 10^{10} M_\odot$.
2. The scatter in the $M_{BH}-M_{star}$ relation is tied to the BH primary growth mode and likely to the initial growth environment. BHs that end up in the bottom quartile in M_{BH} by $z = 0.05$ (undermassive BHs) have experienced almost no BH mergers and instead grow primarily through low accretion rates. BHs that end up in the top quartile (overmassive BHs) experience at least one BH merger and undergo more accretion. Although overmassive BHs accrete more than their undermassive BH counterparts, BHs in dwarf galaxies grow little relative to those found in massive galaxies.
3. The efficiency of BH growth within dwarf galaxies depends on the host formation history, though the difference is most pronounced in galaxies with $M_{star} > 10^9 M_\odot$. Hosts of overmassive BHs rapidly build up dark matter and stars and experience suppression of star formation in their central regions around $z = 2$. By $z = 0.05$, hosts of overmassive BHs have a lower central density of stars than their undermassive BH counterparts. Undermassive BH hosts and galaxies without BHs build up their stars and dark matter nearly identically, suggesting that undermassive BHs do not significantly alter the properties of their host galaxies.
4. Above $M_{star} > 10^9 M_\odot$, quenching of star formation only occurs in galaxies that host BHs, and the majority of such galaxies host an overmassive BH. Overmassive BH hosts show significantly lower levels of H I gas content, regardless of stellar mass, relative to undermassive BH hosts. Further, hosts of overmassive BHs exhibit higher fractions of BH to SN energy injection than undermassive BH hosts, suggesting that overmassive BHs have significant impact on the evolution of dwarf galaxies.

A substantial fraction (~40%) of the BHs in our low-mass galaxy sample grow via mergers with other BHs and exhibit little total growth by accretion. Overall, our results depict a view of BH seeds forming in low-mass galaxies that do not foster efficient gas accretion very frequently. Consequently, the most efficient way to grow BHs in many small galaxies is through mergers with other BHs. Once a galaxy becomes large enough to have a deeper potential well, BH growth by gas accretion may happen more efficiently. Tests of the multiple early BH mergers found in ROMULUS25 will be done in the future by the Laser Interferometric Space Antenna, which will detect BH–BH mergers with total masses $10^4 - 10^7 M_\odot$ up to $z \sim 20$ with good signal-to-noise ratio (Amaro-Seoane et al. 2017).

ORCID iDs

Ray S. Sharma ⓘ https://orcid.org/0000-0001-8350-4535
Alyson M. Brooks ⓘ https://orcid.org/0000-0002-0372-3736
Michael Tremmel ⓘ https://orcid.org/0000-0002-4353-0306
Jillian Bellovary ⓘ https://orcid.org/0000-0001-7596-8372

References

Abraham, R. G., & van Dokkum, P. G. 2014, PASP, 126, 55
Agarwal, B., Vecchia, C. D., Johnson, J. L., Khochfar, S., & Paardekooper, J. P. 2014, MNRAS, 443, 648
Ahn, C. P., Seth, A. C., Cappellari, M., et al. 2018, ApJ, 858, 102
Amaro-Seoane, P., Audley, H., Babak, S., et al. 2017, arXiv:1702.00786
Anglés-Alcázar, D., Faucher-Giguère, C. A., Quataert, E., et al. 2017, MNRAS, 472, L109
Baldassare, V. F., Geha, M., & Greene, J. 2018, ApJ, 868, 152
Baldassare, V. F., Geha, M., & Greene, J. 2020, ApJ, 896, 10
Baldassare, V. F., Reines, A. E., Gallo, E., & Greene, J. E. 2015, ApJL, 809, L14
Baldassare, V. F., Reines, A. E., Gallo, E., & Greene, J. E. 2017, ApJ, 850, 196
Barai, P., & de Gouveia Dal Pino, E. M. 2019, MNRAS, 487, 5549
Barro, G., Faber, S. M., Koo, D. C., et al. 2017, ApJ, 840, 47
Barro, G., Faber, S. M., Pérez-González, P. G., et al. 2013, ApJ, 765, 104
Barth, A. J., Pancoast, A., Thorman, S. J., et al. 2011, ApJL, 743, L4
Begelman, M. C., Volonteri, M., & Rees, M. J. 2006, MNRAS, 370, 289
Bellovary, J. M., Cleary, C. E., Munshi, F., et al. 2019, MNRAS, 482, 2913
Booth, C. M., & Schaye, J. 2009, MNRAS, 398, 53
Bradford, J. D., Geha, M. C., Greene, J. E., Reines, A. E., & Dickey, C. M. 2018, ApJ, 861, 50
Bregman, J. N., Alves, G. C., Miller, M. J., & Hodges-Kluck, E. 2015, JATIS, 1, 045003
Cannon, J. M., Giovanelli, R., Haynes, M. P., et al. 2011, ApJL, 739, L22
Catinella, B., Saintonge, A., Janowiecki, S., et al. 2018, MNRAS, 476, 875
Chandrasekhar, S. 1943, ApJ, 97, 255
Chen, C.-T. J., Brandt, W. N., Reines, A. E., et al. 2017, ApJ, 837, 48
Chen, Z., Faber, S. M., Koo, D. C., et al. 2019, arXiv:1909.10817
Cheung, E., Faber, S. M., Koo, D. C., et al. 2012, ApJ, 760, 131
Choi, E., Ostriker, J. P., Naab, T., et al. 2016, ApJ, 844, 31
Choi, E., Ostriker, J. P., Naab, T., Oser, L., & Moster, B. P. 2015, MNRAS, 449, 4105
Choi, E., Somerville, R. S., Ostriker, J. P., Naab, T., & Hirschmann, M. 2018, ApJ, 866, 91
Colpi, M., Mayer, L., & Governato, F. 1999, ApJ, 525, 720
Covington, M. D., Primack, J. R., Porter, L. A., et al. 2011, MNRAS, 415, 3135

Dashyan, G., Silk, J., Mamon, G. A., Dubois, Y., & Hartwig, T. 2018, MNRAS, 473, 5698
Davis, B. L., Graham, A. W., & Cameron, E. 2018, ApJ, 869, 113
Dekel, A., Ishai, G., Dutton, A. A., & Maccio, A. V. 2017, MNRAS, 468, 1005
Denney, K. D., Peterson, B. M., Pogge, R. W., et al. 2010, ApJ, 721, 715
Diamond-Stanic, A. M., Moustakas, J., Tremonti, C. A., et al. 2012, ApJL, 755, L26
Dickey, C. M., Geha, M., Wetzel, A., & El-Badry, K. 2019, ApJ, 884, 180
Fabian, A. C. 2012, ARA&A, 50, 455
Fan, L., Lapi, A., De Zotti, G., & Danese, L. 2008, ApJL, 689, L101
Franx, M., van Dokkum, P. G., Schreiber, N. M. F., et al. 2008, ApJ, 688, 770
Geha, M., Blanton, M. R., Yan, R., & Tinker, J. L. 2012, ApJ, 757, 85
Governato, F., Brook, C. B., Brooks, A. M., et al. 2009, MNRAS, 398, 312
Governato, F., Weisz, D., Pontzen, A., et al. 2015, MNRAS, 448, 792
Graham, A. W., & Soria, R. 2019, MNRAS, 484, 794
Graham, A. W., Soria, R., & Davis, B. L. 2019, MNRAS, 484, 814
Greene, J. E. 2012, NatCo, 3, 1304
Greene, J. E., Barth, A., Bellini, A., et al. 2019, arXiv:1903.08670
Groves, B. A., Heckman, T. M., & Kauffmann, G. 2006, MNRAS, 371, 1559
Guedes, J., Callegari, S., Madau, P., & Mayer, L. 2011, ApJ, 742, 76
Guo, Y., Ferguson, H. C., Giavalisco, M., et al. 2013, ApJS, 207, 24
Habouzit, M., Genel, S., Somerville, R. S., et al. 2019, MNRAS, 484, 4413
Habouzit, M., Volonteri, M., & Dubois, Y. 2017, MNRAS, 468, 3935
Haiman, Z. 2013, ASSL, 396, 293
Haynes, M. P., Giovanelli, R., Martin, A. M., et al. 2011, AJ, 142, 170
Heckman, T. M., & Best, P. N. 2014, ARA&A, 52, 589
Hilz, M., Naab, T., & Ostriker, J. P. 2013, MNRAS, 429, 2924
Hirschmann, M., Dolag, K., Saro, A., et al. 2014, MNRAS, 442, 2304
Hopkins, P. F., Hernquist, L., Cox, T. J., Younger, J. D., & Besla, G. 2008, ApJ, 688, 757
Hosokawa, T., Yorke, H. W., Inayoshi, K., Omukai, K., & Yoshida, N. 2013, ApJ, 778, 178
Johnson, J. L., Whalen, D. J., Fryer, C. L., & Li, H. 2012, ApJ, 750, 66
Karachentsev, I. D., & Makarov, D. I. 1999, in IAU Symp. 186, Galaxy Interactions at Low and High Redshift, ed. J. E. Barnes & D. B. Sanders (Dordrecht: Kluwer), 109
Kazantzidis, S., Mayer, L., Colpi, M., et al. 2005, ApJL, 623, L67
Kelly, B. C., & Shen, Y. 2013, ApJ, 764, 45
Kennicutt, R. C., Jr+, Tamblyn, P., & Congdon, C. E. 1994, ApJ, 435, 22
Kewley, L. J., Dopita, M. A., Leitherer, C., et al. 2013, ApJ, 774, 100
Knollmann, S. R., & Knebe, A. 2009, ApJS, 182, 608
Kormendy, J., Fisher, D. B., Cornell, M. E., & Bender, R. 2009, ApJS, 182, 216
Kormendy, J., & Ho, L. C. 2013, ARA&A, 51, 511
Kormendy, J., & Richstone, D. 1995, ARA&A, 33, 581
Koudmani, S., Sijacki, D., Bourne, M. A., & Smith, M. C. 2019, MNRAS, 484, 2047
Kravtsov, A. V., Vikhlinin, A. A., & Meshcheryakov, A. V. 2018, AstL, 44, 8
Krolik, J. H. 2001, ApJ, 551, 72
Kroupa, P. 2001, MNRAS, 322, 231
Lemons, S. M., Reines, A. E., Plotkin, R. M., Gallo, E., & Greene, J. E. 2015, ApJ, 805, 12
Li, Y., Habouzit, M., Genel, S., et al. 2020, ApJ, 895, 102
Liu, H.-Y., Yuan, W., Dong, X.-B., et al. 2018, ApJS, 235, 40
Macciò, A. V., Dutton, A. A., & van den Bosch, F. C. 2008, MNRAS, 391, 1940
Madau, P., & Haardt, F. 2015, ApJL, 813, L8
Manzano-King, C. M., Canalizo, G., & Sales, L. V. 2019, ApJ, 884, 54
Martín-Navarro, I., & Mezcua, M. 2018, ApJL, 855, L20
Menon, H., Wesolowski, L., Zheng, G., et al. 2015, ComAC, 2, 1
Mezcua, M., Civano, F., Marchesi, S., et al. 2018, MNRAS, 478, 2576
Mezcua, M., Suh, H., & Civano, F. 2019, MNRAS, 488, 685
Miller, B. P., Gallo, E., Greene, J. E., et al. 2015, ApJ, 799, 98
Milosavljević, M., & Merritt, D. 2001, ApJ, 563, 34
Moran, E. C., Shahinyan, K., Sugarman, H. R., Vélez, D. O., & Eracleous, M. 2014, AJ, 148, 136

Moster, B. P., Naab, T., & White, S. D. M. 2013, MNRAS, 428, 3121
Munshi, F., Governato, F., Brooks, A. M., et al. 2013, ApJ, 766, 56
Nelson, D., Pillepich, A., Springel, V., et al. 2019, MNRAS, 490, 3234
Nguyen, D. D., den Brok, M., Seth, A. C., et al. 2020, ApJ, 892, 68
Nguyen, D. D., Seth, A. C., den Brok, M., et al. 2017, ApJ, 836, 237
Nguyen, D. D., Seth, A. C., Neumayer, N., et al. 2018, ApJ, 858, 118
Nguyen, D. D., Seth, A. C., Neumayer, N., et al. 2019, ApJ, 872, 104
Nipoti, C., Treu, T., Auger, M. W., & Bolton, A. S. 2009, ApJL, 706, L86
Obreschkow, D., & Glazebrook, K. 2014, ApJ, 784, 26
Oser, L., Naab, T., Ostriker, J. P., & Johansson, P. H. 2012, ApJ, 744, 63
Pardo, K., Goulding, A. D., Greene, J. E., et al. 2016, ApJ, 831, 203
Penny, S. J., Masters, K. L., Smethurst, R., et al. 2018, MNRAS, 476, 979
Penny, S. J., Masters, K. L., Weijmans, A.-M., et al. 2016, MNRAS, 462, 3955
Pfister, H., Lupi, A., Capelo, P. R., et al. 2017, MNRAS, 471, 3646
Planck Collaboration, Ade, P., Aghanim, N., et al. 2014, A&A, 571, A16
Pontzen, A., Roškar, R., Stinson, G., & Woods, R. 2013, pynbody: N-Body/ SPH analysis for python, Astrophysics Source Code Library, ascl:1305.002
Pontzen, A., & Tremmel, M. 2018, ApJS, 237, 23
Pontzen, A., Tremmel, M., Roth, N., et al. 2017, MNRAS, 465, 547
Porter, L. A., Somerville, R. S., Primack, J. R., & Johansson, P. H. 2014, MNRAS, 444, 942
Rantala, A., Johansson, P. H., Naab, T., Thomas, J., & Frigo, M. 2018, ApJ, 864, 113
Rantala, A., Pihajoki, P., Johansson, P. H., et al. 2017, ApJ, 840, 53
Reines, A., & Comastri, A. 2016, PASA, 33, e054
Reines, A. E., Condon, J. J., Darling, J., & Greene, J. E. 2020, ApJ, 888, 36
Reines, A. E., Greene, J. E., & Geha, M. 2013, ApJ, 775, 116
Reines, A. E., & Volonteri, M. 2015, ApJ, 813, 82
Ricarte, A., & Natarajan, P. 2018, MNRAS, 481, 3278
Ricarte, A., Tremmel, M., Natarajan, P., & Quinn, T. 2019, MNRAS, 489, 802
Sahu, N., Graham, A. W., & Davis, B. L. 2019, ApJ, 887, 10
Schaye, J., Crain, R. A., Bower, R. G., et al. 2015, MNRAS, 446, 521
Schleicher, D. R. G., Palla, F., Ferrara, A., Galli, D., & Latif, M. 2013, A&A, 558, A59
Schramm, M., & Silverman, J. D. 2013, ApJ, 767, 13
Schutte, Z., Reines, A. E., & Greene, J. E. 2019, ApJ, 887, 245
Shankar, F., Bernardi, M., Sheth, R. K., et al. 2016, MNRAS, 460, 3119
Shen, S., Wadsley, J., & Stinson, G. 2010, MNRAS, 407, 1581
Shen, Y., & Kelly, B. C. 2012, ApJ, 746, 169
Shields, J. C., Walcher, C. J., Böker, T., et al. 2008, ApJ, 682, 104
Sijacki, D., Vogelsberger, M., Genel, S., et al. 2014, MNRAS, 452, 575
Silk, J. 2017, ApJL, 839, L13
Somerville, R. S., & Davé, R. 2015, ARA&A, 53, 51
Springel, V., Pakmor, R., Pillepich, A., et al. 2018, MNRAS, 475, 676
Stinson, G., Seth, A., Katz, N., et al. 2006, MNRAS, 373, 1074
Tremmel, M., Governato, F., Volonteri, M., Pontzen, A., & Quinn, T. R. 2018, ApJL, 857, L22
Tremmel, M., Governato, g. F., Volonteri, M., & Quinn, T. R. 2015, MNRAS, 451, 1868
Tremmel, M., Karcher, M., Governato, F., et al. 2017, MNRAS, 470, 1121
Tremmel, M., Quinn, T. R., Ricarte, A., et al. 2019, MNRAS, 483, 3336
Trujillo-Gomez, S., Klypin, A., Colín, P., et al. 2015, MNRAS, 446, 1140
Trump, J. R., Impey, C. D., Kelly, B. C., et al. 2011, ApJ, 733, 60
van Dokkum, P. G., Bezanson, R., van der Wel, A., et al. 2014, ApJ, 791, 45
Volonteri, M. 2012, Sci, 337, 544
Volonteri, M., Dubois, Y., Pichon, C., & Devriendt, J. 2016, MNRAS, 460, 2979
Volonteri, M., & Natarajan, P. 2009, MNRAS, 400, 1911
Wadsley, J., Stadel, J., & Quinn, T. 2004, NewA, 9, 137
Wadsley, J. W., Keller, B. W., & Quinn, T. R. 2017, MNRAS, 471, 2357
Wadsley, J. W., Veeravalli, G., & Couchman, H. M. P. 2008, MNRAS, 387, 427
Weinberger, R., Springel, V., Hernquist, L., et al. 2017, MNRAS, 465, 3291
Wetzel, A. R., Tinker, J. L., & Conroy, C. 2012, MNRAS, 424, 232
Yuan, W., Zhou, H., Dou, L., et al. 2014, ApJ, 782, 55
Zhao, D. H., Jing, Y. P., Mo, H. J., & Börner, G. 2009, ApJ, 707, 354

16